Quaternary Science Reviews 325 (2024) 108464

Contents lists available at ScienceDirect

Quaternary Science Reviews

journal homepage: www.elsevier.com/locate/quascirev

Holocene fire dynamics and their climatic controls on the southern Cape coast of South Africa - A 7.2 ka multi-proxy record from the peatland Vankervelsvlei

Paul Strobel [a,*], Theresa Henning [a], Marcel Bliedtner [a], Stella G. Mosher [b], Humay Rahimova [c,d], Torsten Haberzettl [e], Kelly L. Kirsten [f], Eva Lehndorff [c], Mitchell J. Power [b,g], Michael Zech [h], Roland Zech [a]

[a] Institute of Geography, Friedrich Schiller University Jena, Jena, Germany
[b] Department of Geography, University of Utah, Salt Lake City, USA
[c] Soil Ecology, University of Bayreuth, Bayreuth, Germany
[d] Research Unit Environmental Simulation, Institute of Biochemical Plant Pathology, Helmholtz Zentrum München, Oberschleißheim, Germany
[e] Institute for Geography and Geology, University of Greifswald, Greifswald, Germany
[f] Department of Geological Sciences, University of Cape Town, Rondebosch, South Africa
[g] Natural History Museum of Utah, University of Utah, Salt Lake City, USA
[h] Heisenberg Chair of Physical Geography with Focus on Paleoenvironmental Research, Institute of Geography, Technische Universität Dresden, Dresden, Germany

ARTICLE INFO

Handling Editor: Dr P Rioual

Keywords:
Paleofire
Paleoclimate
Charcoal
Polycyclic aromatic hydrocarbons
Stable isotopes
Precipitation
Relative humidity

ABSTRACT

Fire is a natural phenomenon along South Africa's southern Cape coast, but identifying its climatic drivers has been a subject of considerable debate. This study investigates the hydroclimatic and fire dynamics from a 9.6 m sediment core from Vankervelsvlei covering the past 7.2 ka. The fen is located near the southern Cape coast within the year-round rainfall zone of South Africa. A reconstruction of hydroclimatic variability through time applies oxygen isotopes from hemicellulose-derived sugars and hydrogen isotopes from leaf wax-derived *n*-alkanes. Coupling both isotopes enables a reconstruction of the atmospheric source and seasonality of precipitation as well as estimating local relative humidity. Past trends in fire activity are inferred from macro-charcoal and polycyclic aromatic hydrocarbon (PAH) analyses, the latter serving as fire biomarkers.

Results indicate high fire activity at Vankervelsvlei accompanied by generally moist conditions and a year-round rainfall regime linked to both Westerly-derived winter precipitation and Easterly- and locally-derived summer precipitation from $7.2^{+0.2}/_{-0.2}$ to $4.5^{+0.3}/_{-0.3}$ cal ka BP. From $4.5^{+0.3}/_{-0.3}$ to $1.5^{+0.4}/_{-0.2}$ cal ka BP, a shift to a Westerly-derived winter rainfall regime is identified. This variation features alongside reduced fire activity and persistent drought conditions as Easterly- and locally-derived summer precipitation decreased. From $1.5^{+0.4}/_{-0.2}$ cal ka BP until present day, macro-charcoal and PAH accumulation rates show high fire activity. Paleoclimate evidence from the last two millennia suggests a variable climate with an overall increase in total moisture availability as contributions from both Westerly-derived winter precipitation and Easterly- and locally-derived summer precipitation support the year-round rainfall regime present today.

Results from Vankervelsvlei support previous evidence from regional paleo-reconstructions, refining our understanding of the interplay between hydroclimatic variability and fire activity along South Africa's southern Cape coast. Our study discusses the role of large-scale climate modes, specifically the intensity of El Niño, as a potential driver of short-term hydroclimatic variability, which in turn drives fuel availability and fire activity at Vankervelsvlei during the Holocene.

* Corresponding author.
E-mail address: paul.strobel@uni-jena.de (P. Strobel).

https://doi.org/10.1016/j.quascirev.2023.108464
Received 30 June 2023; Received in revised form 4 December 2023; Accepted 4 December 2023
Available online 2 January 2024

1. Introduction

Wildfires are a common natural phenomenon in many regions of South Africa promoting biodiversity and ecosystem productivity (Archibald et al., 2009; Bond et al., 2003; Finch et al., 2022; Kraaij and van Wilgen, 2014). Today, southern Africa's climate is driven by the interaction between oceanic circulation systems, including the cold Benguela Current on the west coast and warm Agulhas Current along the east and south coasts, and atmospheric circulation, leading to the presence of three major rainfall seasonality zones (Fig. 1B) (Haberzettl et al., 2014; Tyson and Preston-Whyte, 2000; van Zinderen Bakker, 1976). The eastern and central parts of the country experience the majority of their rainfall during austral summer (summer rainfall zone, SRZ). Summer precipitation originates from tropical moisture bearing atmospheric circulation systems (i.e. Easterlies) with the Indian Ocean as the moisture source (Geppert et al., 2022; Tyson and Preston-Whyte, 2000). The country's west coast receives most of its precipitation during the austral winter (winter rainfall zone, WRZ). Winter precipitation is supplied by temperate westerly winds (i.e. Westerlies) with the Atlantic Ocean as the source of moisture (Geppert et al., 2022). An intermediate area between the SRZ and WRZ receives rainfall from both systems throughout the year and is identified as the year-round rainfall zone (YRZ) (Fig. 1 B) (Engelbrecht et al., 2015; Scott and Lee-Thorp, 2004), which includes the relatively humid southern Cape coast, where this study is located (Fig. 1B).

Numerous studies investigated Mid and Late Holocene paleoclimatic dynamics in the YRZ using methods from disciplines such as palynology and paleontology as well as organic, inorganic, and stable isotope geochemistry (du Plessis et al., 2021a; du Plessis et al., 2021b; Kirsten et al., 2018; Quick et al., 2015; Quick et al., 2018; Strobel et al., 2021; Strobel et al., 2022b; Wündsch et al., 2018). Considering chronological uncertainties, results indicate moist conditions from 7.5 to 5.0 cal ka BP, rather dry conditions from 5.0 to 3.0 cal ka BP followed by increasing moisture from 3.0 cal ka BP until the present day along the southern Cape coast. However, those studies often lack precise chronological control, are discontinuous or confined to specific periods, and/or have low temporal resolution.

Paleofire records from each rainfall zone highlight the presence of two different fire regimes in South Africa, i.e. a western and an eastern fire stack (Davies et al., 2022). The frequency of fires in the WRZ and YRZ (western fire stack) appears to be in antiphase to the SRZ (eastern fire stack) for much of the Holocene. Particularly, the western fire stack shows high fire activity from 7.2 to 4.5 cal ka BP, cal ka low fire activity from 4.5 to 2.0 cal ka BP, and an increasing trend since 2.0 cal ka BP. Conversely, the eastern fire stack indicates low fire activity from 7.5 to 4.5 cal ka BP and from 3.0 to 2.0 cal ka BP, high fire activity from 4.5 to 3.0 ka but also reveals an increasing trend from 2.0 cal ka BP to present (Davies et al., 2022). This pattern is linked to changes in temperature, precipitation, and relative humidity which influences the type, amount, and arrangement of vegetation-fuel characteristics in each region (Duane et al., 2021; Kraaij and van Wilgen, 2014; Power et al., 2008). However, both regional fire histories show an increasing presence of human-caused fires during the past two millennia (Davies et al., 2022).

Understanding the role of fire and hydroclimate variability in the YRZ in relation to the region's biodiversity is critically important, especially considering the growing evidence of regional climate sensitivity (Kraaij and van Wilgen, 2014; Strobel et al., 2022b; van Zinderen Bakker, 1978). For example, in the Fynbos biome, which covers large areas in the region, fires are a natural phenomenon and the biome's presence depends on frequent wildfire activity (Kraaij et al., 2018; Kraaij and van Wilgen, 2014; Ziervogel et al., 2014). However, as a result of rising temperatures and higher drought frequency linked to climate change, the number of large and destructive wildfires has increased. This trend became apparent in 2017 as fires burned 15,000 ha near the

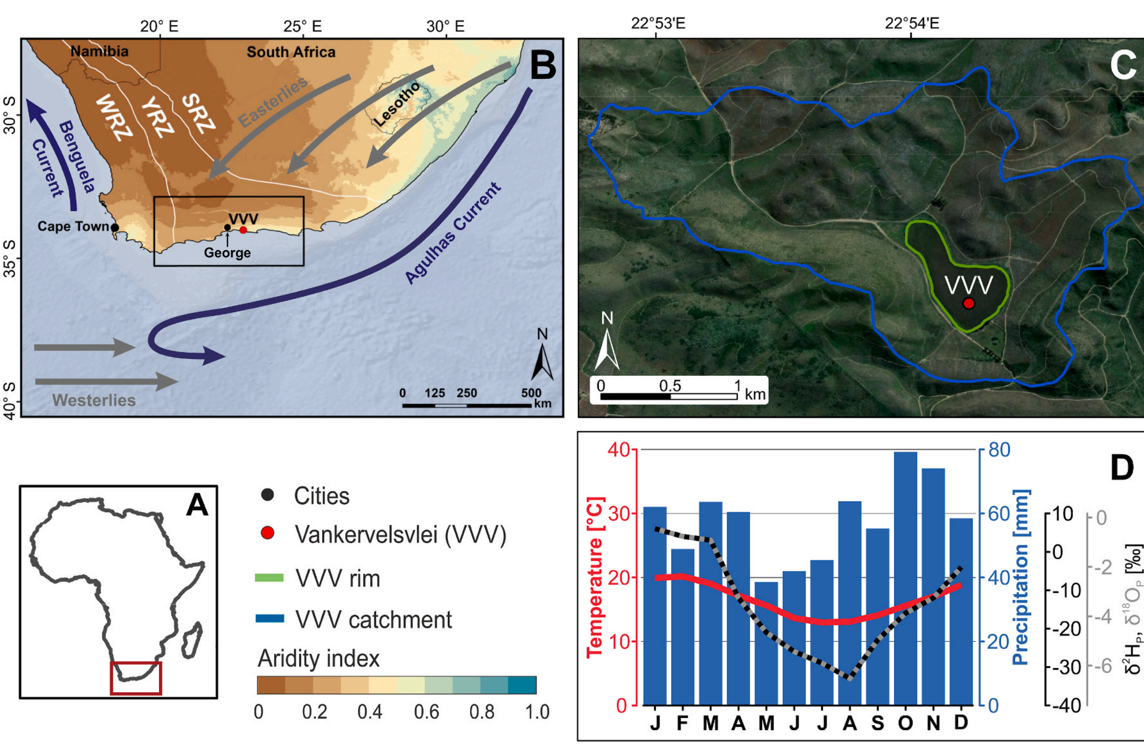

Fig. 1. **A**) Simplified map of Africa. The red box is magnified in B. **B**) Location of Vankervelsvlei (red dot, labeled VVV) and the three major rainfall zones of South Africa, i.e. winter-rainfall zone (WRZ), year-round rainfall zone (YRZ) and summer rainfall zone (SRZ) after Chase and Meadows (2007) derived from Worldclim 2 dataset (Fick and Hijmans, 2017). Additionally, the circumpolar Westerlies, the tropical Easterlies, the Agulhas Current, the Benguela Current, and the Aridity Index (brown to green color, Zomer et al., 2022) are depicted. **C**) Topographic map (ESRI Inc., 2020) including catchment and rim of Vankervelsvlei as well as the coring position. **D**) Climate diagram illustrating the seasonal variability of precipitation and temperature (1981–2020; Station: George Airport; DWD Climate Data Center, 2020) as well as the variability of δ^2H_p and $\delta^{18}O_p$ (Bowen, 2022; Bowen et al., 2005) at Vankervelsvlei. The figure was modified after Strobel et al. (2022b).

urban centers of Knysna, Sedgefield, and Plettenberg Bay (Frost et al., 2018; Kraaij et al., 2018) (Fig. 2). Large destructive fires are predicted to increase in the region due to future climate change (Duane et al., 2021; IPCC, 2021; Wilson et al., 2010; Ziervogel et al., 2014), but there is a lack of understanding of past fire dynamics and their environmental drivers along the southern Cape coast. To some degree, this is attributed to the limited number of paleofire records in the area and previous fire history records that offer a low temporal resolution, discontinuous or poor chronologies of fire and often target specific periods in the past (e.g. du Plessis et al., 2020; du Plessis et al., 2021a; Quick et al., 2015; Quick et al., 2016). Additionally, a comprehensive understanding of the complex atmospheric forcing over South Africa and the southern Cape coast is still evolving (e.g. Sjöström et al., 2023; Strobel et al., 2022b; Wündsch et al., 2018). Current paleofire reconstructions along South Africa's southern Cape coast are primarily sedimentary charcoal-based fire histories, with few studies exploring site-specific linkages between fire activity and climate dynamics during the Holocene (e.g. du Plessis et al., 2020; du Plessis et al., 2021b; MacPherson et al., 2019; Quick et al., 2015; Quick et al., 2018; Quick et al., 2016). Therefore, multi-dimensional studies are essential to gain a more comprehensive understanding of past fire dynamics and its climatic controls along the southern Cape.

Besides well-established and widely used macro-charcoal analyses (Conedera et al., 2009; Finch et al., 2022; Norström et al., 2014),

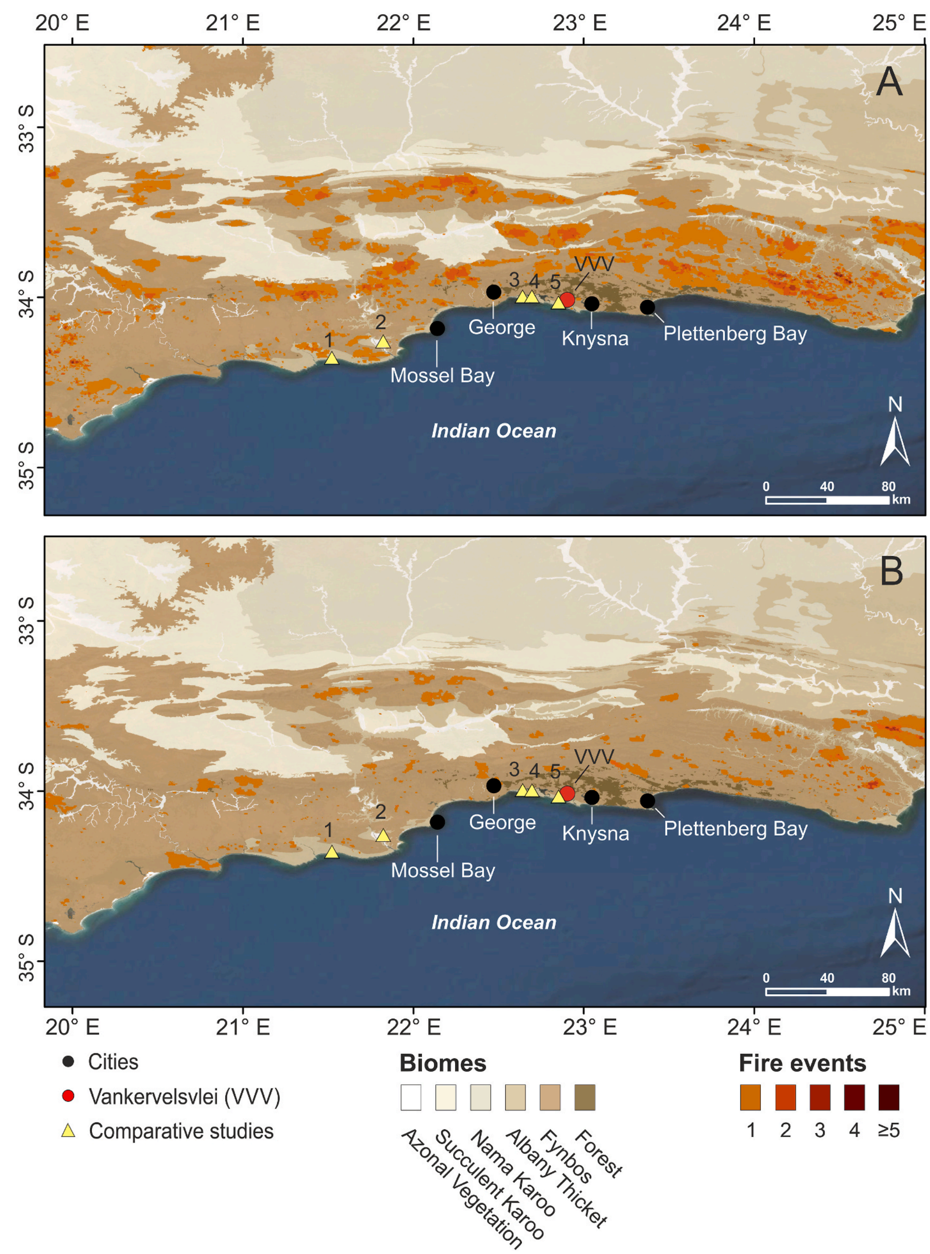

Fig. 2. Modern fire seasonality on the southern Cape coast for the period from 2003 to 2016, with **A)** showing the area burnt in the summer period (from October to March), and **B)** in the winter period (from April to September). The area burnt is classified into fire events (from one to a maximum of six) for the respective seasons, based on the Global Fire Atlas algorithm and estimations of the day of burn information at 500 × 500 m resolution (0.25 km^2) from the Moderate Resolution Imaging Spectroradiometer (MODIS) Collection 6 MCD64A1 burned area product (Andela et al., 2019). Further depicted are the major biomes on the southern Cape coast after Mucina and Rutherford (2006), showing increased fire activity in the Fynbos biome. In addition, the location of Vankervelsvlei (red dot, labeled VVV) and paleoenvironmental records covering the Holocene are indicated: 1) Rietvlei-Still Bay (Quick et al., 2015), 2) Voëlvlei (Strobel et al., 2021), 3) Eilandvlei (du Plessis et al., 2021a; Kirsten et al., 2018; Quick et al., 2018; Wündsch et al., 2018), 4) Bo Langvlei (du Plessis et al., 2020), 5) Groenvlei (Martin, 1968; Wündsch et al., 2016). Oceanic map was used from ESRI Inc. (2022).

molecular biomarkers such as polycyclic aromatic hydrocarbons (PAH) have been established as tools for reconstructing past fire dynamics (Denis et al., 2012; Karp et al., 2020; Sjöström et al., 2023; Vachula et al., 2022). PAHs are characterized by multiple aromatic rings originating from incomplete combustion of organic matter, which can stay well-preserved in soils and sediments (e.g. Argiriadis et al., 2018; Callegaro et al., 2018; Conedera et al., 2009; Karp et al., 2021). The chemical structure of fire-derived PAH compounds allows inferring, for example, PAH source, burn phase or burn temperature (Denis et al., 2012; Karp et al., 2020; McGrath et al., 2003). Although the number of studies using PAHs is limited compared to macro-charcoal applications, the few existing studies have shown the potential of PAHs for reconstructing past fire dynamics in different regions of the world (e.g. Bandowe et al., 2014; Battistel et al., 2016; Callegaro et al., 2018; Vachula et al., 2022).

On the other hand, paleofire dynamics are highly linked to global and regional climatic conditions (e.g. Kraaij et al., 2022; Power et al., 2008; Sjöström et al., 2023) and stable isotope analyses have shown enormous potential for providing paleoclimatic reconstructions. Current and previous isotope research has identified significant contributions toward understanding paleohydrological changes in South Africa (e.g. Miller et al., 2019; Strobel et al., 2021; Strobel et al., 2022b; Strobel et al., 2020). Coupling hydrogen isotopes from leaf wax-derived *n*-alkanes ($\delta^2H_{n\text{-alkane}}$) and oxygen isotopes from hemicellulose-derived sugars ($\delta^{18}O_{sugar}$) in a so-called coupled isotope approach (paleohygrometer) assists in disentangling changes in the amount and seasonality of precipitation related to the atmospheric source of precipitation and local relative humidity (Hepp et al., 2021; Lemma et al., 2021; Strobel et al., 2020, 2022b). This approach has already been regionally calibrated in South Africa (Strobel et al., 2020) and successfully applied to sediments from Vankervelsvlei, with the current study significantly expanding the temporal resolution of previous work (Strobel et al., 2022b).

In this study, a combined approach of well-established macro-charcoal and innovative PAH analyses is applied to robustly reconstruct the Holocene fire history at Vankervelsvlei located on South Africa's southern Cape coast. Additional $\delta^{18}O_{sugar}$ analyses were carried out to complement the available $\delta^2H_{n\text{-alkane}}$ and $\delta^{18}O_{sugar}$ records by Strobel et al. (2022b) in order to gain a comprehensive picture of the past environmental and in particular hydrological conditions in this area at high temporal resolution. Using a multi-proxy approach, this study aims at i) evaluating the potentials and limitations of macro-charcoal and PAH analyses for paleofire reconstruction at Vankervelsvlei; ii) assessing past changes in the local and regional fire dynamics, i.e. occurrence, frequency, and fuel condition; and iii) identifying potential climatic drivers of past fire dynamics for the past 7.2 ka at a multi-decadal resolution. Considered together with existing paleofire records from the southern Cape coast, this research contributes to a more comprehensive understanding of paleoenvironmental changes and respective ecosystem responses throughout the Holocene.

2. Material and methods

2.1. Study site

Vankervelsvlei is a peatland situated at an elevation of 152 m a.s.l. on the southern Cape coast of South Africa located about 400 km east of Cape Town, 40 km east of George, and 5 km inland of the present coast (Fig. 1B). Vankervelsvlei is an irregular shaped endorheic depression enclosed by cemented coastal dunes of Late Quaternary age (250–205 ka; Bateman et al., 2011; Illenberger, 1996), that separate the peatland from the present coast. Soils in the region are typically acidic, leached, shallow, and nutrient deficient (e.g. Alisols and Luvisols) (Geldenhuys, 1988; Irving and Meadows, 1997). The peatland itself comprises an area of 0.34 km^2, with a maximal length of 800 m and a maximal width of 460 m. Vankervelsvlei receives most of its water from direct precipitation and water quickly penetrates through the sand dunes (Mandiola et al., 2021). The catchment has an area of 4.1 km^2 (Fig. 1C) (Database: SRTM 1 arc-second; NASA, 2013; Strobel et al., 2022b).

Mean annual precipitation at George Airport is 690 mm•yr $^{-1}$ but has become highly variable during recent years, without significant seasonality (ranging from 375 to 1220 mm•yr^{-1}; 1981–2020) (DWD Climate Data Center, 2020). The stable hydrogen and oxygen isotopic composition of precipitation (δ^2H_p, $\delta^{18}O_p$) reflects the contribution of different precipitation systems (Braun et al., 2017; Geppert et al., 2022; Harris et al., 2010). During winter, precipitation originates from the Atlantic Ocean (Westerlies) and is ^{2}H- and ^{18}O-depleted. Conversely, during summer, precipitation originates from the Indian Ocean (Easterlies) and is ^{2}H- and ^{18}O-enriched. Moreover, ridging anticyclones produce onshore flow that leads to orographic ^{2}H- and ^{18}O-enriched rainfall from local sources occurring year-round (Bowen, 2022; Braun et al., 2017; Engelbrecht and Landman, 2016; Geppert et al., 2022; Harris et al., 2010; Weldon and Reason, 2014).

Temperatures in the area are generally uniform with an annual mean of 16.5 °C and a mean monthly maximum in February (20.1 °C) and a minimum in July (12.9 °C) (1981–2020) (DWD Climate Data Center, 2020). South-westerly winds predominate and are coupled with mountain wind conditions, especially in the autumn and winter months, which can periodically result in anomalously high temperatures in the coastal regions of the YRZ (Illenberger, 1996; Quick et al., 2016). As a result of the prevailing environmental conditions, the natural vegetation is a mosaic of floristic species of the Fynbos biome (Mediterranean-climate shrublands), the Albany Thicket biome (dense shrublands including succulent plants), and the Afrotemperate Forest biome (tall trees and a sparse understorey) (Irving, 1998; Kraaij et al., 2018; Mucina and Rutherford, 2006) (Fig. 2). Presently, large areas are also used as commercial pine (*Pinus*) plantations within which the Vankervelsvlei catchment lies. The vegetation growing on the fen predominantly consists of Cyperaceae with some ferns (Pteridophytes) and mosses (Bryophytes) (Quick et al., 2016).

The mean fire return interval in the area has averaged 8–15 years in recent decades and the aseasonal fire regime is consistent with low seasonality of climate controls in terms of precipitation and lightning (Kraaij et al., 2013b; Kraaij and van Wilgen, 2014). Lightning is the primary natural cause of wildfires on the southern Cape occurring throughout the year at an average density of 0.4 km^{-2}•yr^{-1} with slightly lower activity in the winter months (Archibald et al., 2009; Kraaij et al., 2013a; Kraaij and van Wilgen, 2014). Although fires occur throughout the year, and fire danger conditions are generally low to moderate (Kraaij et al., 2013a, 2013b), fire-prone conditions are more elevated from May to August, associated with the mountain wind season (Geldenhuys, 1994; Kraaij et al., 2013a). Hot and dry mountain winds, particularly occurring in the autumn and winter months, cause anomalously elevated temperatures related to an increased fire potential in terms of frequency, severity, and size of fires along the southern Cape coast (Kraaij et al., 2013a). In general, a prolonged annual drought period, combined with a relatively rapid build-up of fuel, favors frequent vegetation fires at lower elevations across the southern Cape (Archibald et al., 2009; Kraaij and van Wilgen, 2014). Consequently, apart from weather conditions and the presence of ignition sources (i.e. lightning), the propensity to burn is influenced by the amount, type, and arrangement of available fuel (Archibald et al., 2009; Kraaij and van Wilgen, 2014). In the Fynbos biome, fires are a natural disturbance agent and are necessary to maintain the ecological status (Kraaij and van Wilgen, 2014; Quick et al., 2016; Ziervogel et al., 2014) (Fig. 2). Although small fires are common, Fynbos fire regimes are predominantly characterized by less frequent large wildfires (Kraaij and van Wilgen, 2014). The Albany Thicket biome and the Afrotemperate forest, however, generally tend to be fire adverse and are restricted to fire-protected sites such as sheltered ravines, stream banks, or berg wind shadows (Geldenhuys, 1994; Kraaij and van Wilgen, 2014; van Wilgen et al., 1990). Nevertheless, they can burn under extreme weather conditions (Kraaij et al., 2018).

At present, however, remote sensing data show a different fire behavior for the southern Cape coast with higher fire occurrence in spring and summer compared to autumn and winter for the period from 2003 to 2016 (Fig. 2). This could be driven by anthropogenic activities, e.g. both starting and preventing fires, as well as the transformation of the natural vegetation to fire-prone pine plantations rather than natural patterns of fire (Kraaij and van Wilgen, 2014). In addition, the effects of climate change, with an increase in fire-favorable weather and droughts in recent years (Kraaij et al., 2013a; Ziervogel et al., 2014), may have already led to changes in the existing fire regimes.

2.2. Vankervelsvlei sediment record

The composite sediment record compilation, chronology, and lithology of the investigated sequence from Vankervelsvlei was described in detail by Strobel et al. (2022b). Three parallel piston cores (UWITEC, Mondsee, Austria), as well as one push core for the uppermost sediments, were retrieved from Vankervelsvlei (34.013° S; 22.904° E) in 2016 (Fig. 1). For this study, we focus on the upper 9.62 m with a modeled basal age of $7230^{+160}/_{-210}$ cal BP (Strobel et al., 2022b) which is based on radiocarbon ages of seven organic macro particles and two bulk organic carbon samples (Fig. 3) (du Plessis et al., 2021b; Strobel et al., 2019).

From 9.62 to 0.8 m composite depth (with a gap from 3.9 to 2 m due to core loss), the sediments consist of peat material of dark brown, reddish to black color, and several macro remains are present in the lower parts (Strobel et al., 2019, 2022b). The uppermost sediments from 0.8 to 0 m composite depth comprise well-preserved organic matter of yellowish to reddish color with the presence of roots and macro remains. For previous organic, inorganic, and stable isotope geochemical analyses (Strobel et al., 2019, 2022b) the composite record was subsampled and freeze-dried in 8 cm intervals. Those samples have now been used for PAH and $\delta^{18}O_{sugar}$ analyses. Subsamples for macro-charcoal analysis originate from slightly different depths but were sampled as close as possible to the aforementioned samples (i.e. 1-2 cm above or below).

2.3. Macro-charcoal analyses

For macro-charcoal analyses, 1 cm sediment slices of 60 samples were freeze-dried (−50 °C, <72 h). An aliquot of the samples was soaked in 5% sodium hexametaphosphate for 24–72 h at the University of Utah (e.g. Long et al., 1998). Sample masses were adjusted based on charcoal content and ranged from 0.03 to 0.88 g dry sediment. The residues were wet-sieved using tap water through nested 250 μm and 125 μm screens to isolate macroscopic charcoal particle size fractions before samples were rinsed into gridded Petri dishes (Conedera et al., 2009). The charcoal in each dish was counted under a stereomicroscope at 20X magnification for 250 μm samples and 36X magnification for 125 μm samples. Charcoal fragments were identified by their color, morphology, and texture. Unfortunately, we are not able to report fluxes for our charcoal data, because we only measured the weight but not the volume of the samples. However, we normalized our charcoal fragments to the sample weight and the time span encompassed in the 1 cm sediment slice used for analyses. Sedimentation rates are derived from the Bayesian age-depth model by Strobel et al. (2022b). Charcoal data are therefore shown as accumulation rates (#particles•g^{-1}•yr^{-1}) in order to overcome potential biases due to variation is sediment properties (e.g., variations in density or sediment accumulation rate) (e.g. Vachula et al., 2018). We note that the charcoal record refers to local fire activity rather than regional fire activity due to limited land mass surrounding the coastal site, including mountainous terrain to the north, and the size classes chosen (e.g. Hennebelle et al., 2020; Vachula et al., 2018).

2.4. Polycyclic aromatic hydrocarbons

For PAH analysis, samples were freeze-dried, ground, and homogenized. Seventy one samples (0.3–2.4 g dry sediment) were solvent extracted at the Department of Geography, Friedrich Schiller University Jena, Germany. An ultrasonic bath extraction was conducted with 40 ml dichloromethane (DCM) and methanol (MeOH) (9/1; v/v) over three 15 min cycles to receive the total lipid extracts. After solvent evaporation, the total lipid extracts were separated by solid phase extraction using aminopropyl silica gel (Supelco; 45 μm) as stationary phase into the following fractions: (i) the apolar fraction, (ii) the polar fraction, and (iii) the acid fraction by elution with hexane, DCM:MeOH (1:1; v/v), and DCM:formic acid (98:2; v/v), respectively. After solvent evaporation, the polar fraction was purified over pipette columns filled with deactivated silica in two different mesh sizes (Mechery-Nagel; 15–40 μm and 63–200 μm) following the standard protocol at the BayCEER laboratory at the University of Bayreuth using hexane and DCM:hexane (2:1; v/v). The latter fraction is yielding the aromatic compounds. PAH analyses were conducted by using a gas chromatograph (GC; Agilent Technologies 7890 A, Germany) coupled with a mass spectrometer (MS; Agilent

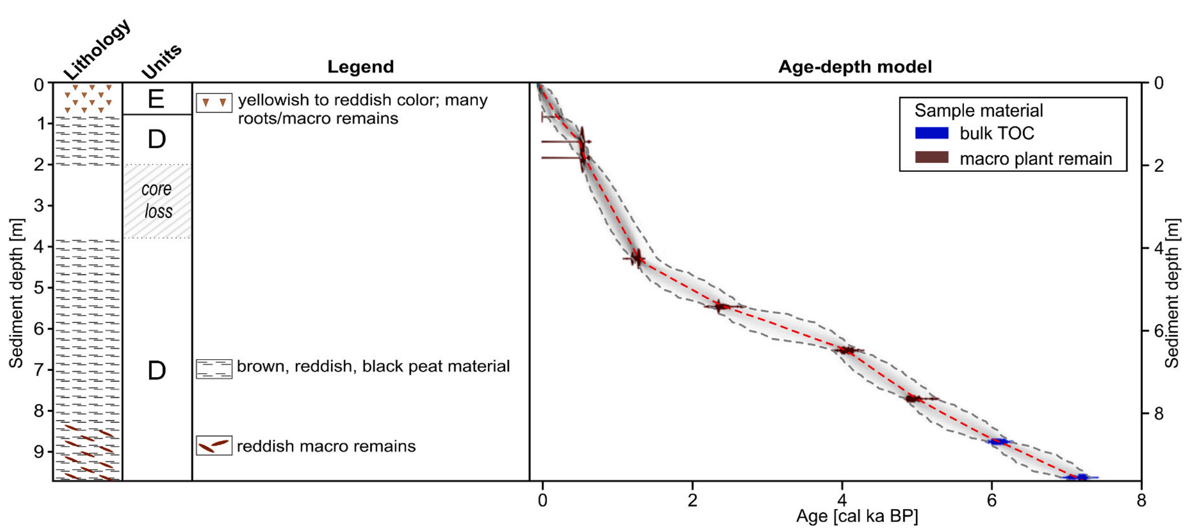

Fig. 3. Lithology, lithological units, and their respective descriptions as well as an age-depth model of the Holocene section of the VVV16 composite record. Calibrated radiocarbon ages are displayed as probability density functions of the 2σ distributions. Age-depth modeling was carried out using the R software package Bacon 2.4.3 (Blaauw and Christen, 2011). The figure is modified after Strobel et al. (2022b).

5975 B Agilent Technologies) at the University of Bayreuth. The GC was equipped with an HP-5MS column (30 m × 250 μm × 0.25 μm). The injector was set to 250 °C, 54 ml•min^{-1} inlet flow, and 9.4 psi pressure on the column. Samples were analyzed by injecting 1 μl in splitless mode (250 °C of Front inlet and Mass Analyzer source temperature). Helium gas was used as a carrier gas and the oven temperature program was set to 80 °C (hold for 2 min), ramped to 250 °C at 10 °C•min^{-1}, and then to 320 °C at 3 °C•min^{-1}. For PAH analysis, the routine limit of quantification as the smallest detectable concentration of the external standard was applied, i.e. 0.01 μg•ml^{-1}. Laboratory blanks were processed with the samples. Ten mass groups of parent and alkyl PAHs were chosen in SIM mode for optimum method development. Precautions against contamination of equipment by PAHs were performed as reported by Bläsing et al. (2016, 2017) with minor modifications. The identification and quantification of the PAHs were performed by comparing the mass spectra with those in the external standard and by the NIST library. The external standards included 16 compounds with high and low molecular weight PAHs (QTM-PAH mix, Sigma-Aldrich, Germany). Mass spectra of perylene and methylated phenanthrenes (3-, 2-, 9-, and 1+4-methylphenanthrene isomers) were additionally confirmed with individual standards and according to retention time as described in Poster et al. (2003). Overall, a total of 8 PAHs were identified and quantified from the Vankervelsvlei sediments, i.e. Phe, MPhe, Flua, Py, BaA, Chr, Per, and BghiP (Table 1), and their respective concentrations are given in ng·g^{-1}. In order to calculate the total PAH concentration of pyrogenic PAHs, the aforementioned compounds were summed up except for Per due to its predominantly biogenic origin (see section 5 for further details). To evaluate PAH sources and changes in fire regimes and fuel source we use diagnostic molecular ratios of components with identical masses, i.e. [Flu/(Flu + Pyr)] and [BaA/(BaA + Chr] (e.g. Kappenberg et al., 2019; Karp et al., 2018; Yunker et al., 2002).

We follow the procedure by Topness et al. (2023) and normalized PAH concentrations to the time span encompassed by the 1 cm sediment slice used for lipid extraction. Sedimentation rates are derived from the Bayesian age-depth model by Strobel et al. (2022b). PAHs are therefore reported as accumulation rates (ng•g^{-1}•yr^{-1}; note that the gram unit included in this accumulation rate refers to the sediment sample weight from which PAHs were extracted and does not reflect the mass or density of the sediment core itself (Topness et al., 2023)). The use of PAH accumulation rates eliminates potential influences of variations in sediment density or sediment accumulation rates, which could bias the PAH interpretation (e.g. Topness et al., 2023; Vachula et al., 2022).

Table 1
PAHs identified from Vankervelsvlei sediments. Compounds with concentrations below detection limit are signalled by (n.d.).

PAHs	Abbreviation	Rings	Targeted ion (m/z)
Phenanthrene	Phe	3	178
Methylphenanthrenes	MPhe	3	192
Fluoranthene	Flua	4	202
Pyrene	Py	4	202
Benz(a)anthracene	BaA	4	228
Chrysene	Chr	4	228
Perylene	Per	5	252
Benzo(g,h,i)perylene	BghiP	6	276
Naphthalene (n.d.)	Nap	2	128
Acenaphthylene (n.d.)	Acy	3	152
Acenaphthene (n.d.)	Ace	3	154
Fluorene (n.d.)	Flo	3	166
Anthracene (n.d.)	Ant	3	178
Retene	Ret	3	234
Benzo[b]fluoranthene (n.d.)	B(b)F	5	252
Benzo[k]fluoranthene (n.d.)	B(k)F	5	252
Benzo[a]pyrene (n.d.)	B(a)P	5	252
Indeno[1,2,3-cd]pyrene (n.d.)	IP	6	276
Dibenz[a,h]anthracene (n.d.)	DB(ah)A	5	278

2.5. Sugar biomarker analyses and coupled isotope approach

For sugar biomarker analyses, samples were freeze-dried, ground, and homogenized. Hemicellulose-derived sugars were hydrolytically extracted from 52 samples (0.2–0.4 g, depending on TOC content) at the Department of Physical Geography at the Friedrich Schiller University Jena. Samples were extracted with 10 ml of 4 M trifluoroacetic acid at 105 °C for 4 h as described in Amelung et al. (1996). Thereafter, samples were vacuum-filtered over glass fiber filters and the extracted sugars were cleaned according to Zech and Glaser (2009) using XAD-7 and Dowex 50WX8 columns to remove humic-like substances and cations. The purified sugar samples were freeze-dried (−50 °C, 24 h) and derivatized with methylboronic acid (1 mg in 100 μl pyridine) at 60 °C for 1 h. Myo-Inositol was used as an internal standard. The compound-specific oxygen isotope measurements were performed at the Institute of Geography at the Technische Universität Dresden using a Trace GC 2000 coupled to a Delta V Advantage IRMS using an ^{18}O-pyrolysis reactor (GC IsoLink) and a ConFlo IV interface (all devices from Thermo Fisher Scientific, Bremen, Germany). Samples were injected in splitless mode and measured in triplicates. For calibration, standard blocks of derivatized sugars (arabinose, fucose, xylose) at various concentrations and known $\delta^{18}O$ values were measured. All $\delta^{18}O_{sugar}$ results were additionally corrected for hydrolytically introduced oxygen atoms which form carbonyl groups within the sugar molecules (Zech and Glaser, 2009). Arabinose and fucose were less abundant compared to xylose and therefore not considered for further data evaluation. The standard deviation of the sugar sample triplicate measurements was <2.1‰. Standard duplicate measurements had a standard deviation of <1.6‰ ($n = 13$). The oxygen isotopic composition is given in the delta notation ($\delta^{18}O$) in per mille versus VSMOW.

The coupled $\delta^2H_{n\text{-alkane}}$–$\delta^{18}O_{sugar}$ approach (paleohygrometer) has previously been described in detail by e.g. Hepp et al. (2015, 2017), Hepp et al. (2019, 2020), Hepp et al. (2021), Lemma et al. (2021) and Tuthorn et al. (2015). The fundamental assumption of the approach is that the isotopic composition of leaf water can be reconstructed by applying biosynthetic fractionation factors (ε_{bio}) on the measured $\delta^2H_{n\text{-alkane}}$ and $\delta^{18}O_{sugar}$ values (Cernusak et al., 2022; Liu et al., 2023). For $\delta^2H_{n\text{-alkane}}$ a constant ε_{bio} value of about −160‰ (Liu and Liu, 2019; Sachse et al., 2012; Sessions et al., 1999) is applied; for $\delta^{18}O_{sugar}$ the ε_{bio} value is assumed to be +27‰ (Cernusak et al., 2003; Gessler et al., 2009; Hepp et al., 2021; Schmidt et al., 2001; Sternberg et al., 1986; Yakir and DeNiro, 1990). This can be illustrated in a δ^2H–$\delta^{18}O$ diagram (Fig. 4) where the distance of the reconstructed leaf water to the global meteoric water line (GMWL) is defined as deuterium-excess (Dansgaard, 1964) (Fig. 4). The concept is furthermore based on the fact that the isotopic composition of precipitation plots typically close to the GMWL ($\delta^2H_p = 8 \cdot {}^{18}O_p + 10$; Dansgaard, 1964). However, on the central southern Cape coast of South Africa, a local meteoric water line (LMWL) slightly deviating from the GMWL was described by Braun et al. (2017) ($\delta^2H = 7.70 \cdot \delta^{18}O + 12.10$) (Fig. 4). This LMWL was used for our calculations. We calculated equilibrium fractionation factors according to Horita and Wesolowski (1994) based on modern MAT, i.e. 16.4 °C (DWD Climate Data Center, 2020), resulting in 82.1‰ for ^{2}H and 10.0‰ for ^{18}O. The kinetic fractionation factor for ^{2}H and ^{18}O is set to 25.1‰ and 28.5‰, respectively (Merlivat, 1978). This yields a specific slope for a local evaporation line (LEL) of 2.78. The intercept of the LEL and the LMWL is the isotopic composition of reconstructed plant-source water (δ^2H and $\delta^{18}O$) (Fig. 4). The difference between deuterium-excess of the reconstructed leaf water and reconstructed plant-source water is then used to estimate the relative humidity (RH) for each sample (Fig. 4). Errors for reconstructed leaf water, plant-source water, d-excess, and estimated RH were calculated using error propagation of the analytical uncertainties of the biomarker analyses ($\delta^2H_{n\text{-alkane}}$, $\delta^{18}O_{sugar}$) and are depicted as error bars in Figs. 6 and 8.

We acknowledge that changes in the vegetation composition could have led to variations in ε_{bio}. Depending on the plant functional type ε_{bio}

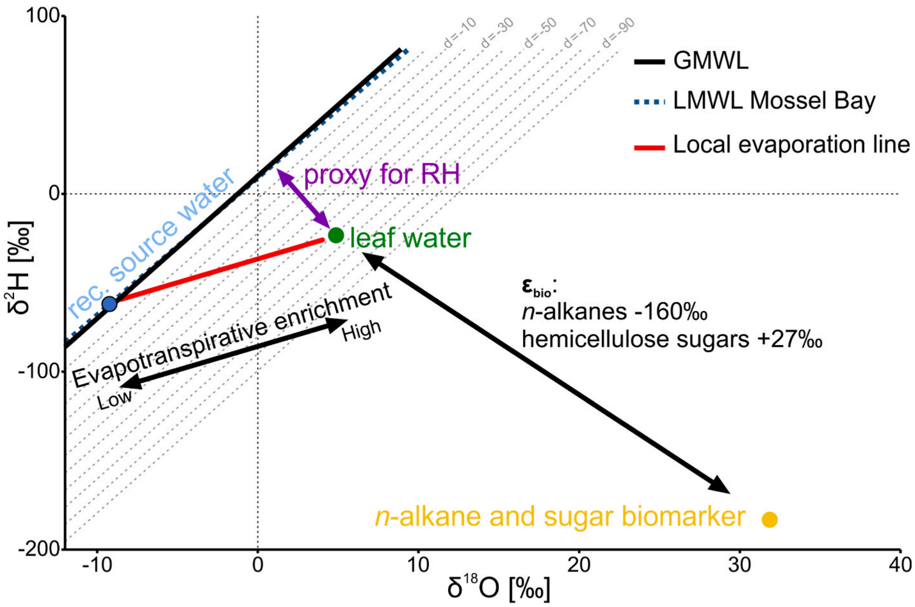

Fig. 4. Conceptual framework of the coupled $\delta^2H_{n\text{-alkane}}$–$\delta^{18}O_{sugar}$ approach (paleohygrometer) displayed as δ^2H–$\delta^{18}O$ diagram showing the isotopic hydrogen and oxygen composition of leaf wax-derived *n*-alkanes and hemicellulose-derived sugars, respectively (after Zech et al., 2013). Additionally depicted are the reconstructed leaf and plant-source water, the global meteoric water line (GMWL, black line), and the local meteoric water line (LWML) from Mossel Bay (blue dashed line; Braun et al., 2017). The black double arrows indicate natural processes of evapotranspirative enrichment of leaf water along the local evaporation line (red line) and biosynthetic fractionation during biomarker synthesis, respectively. Grey dashed lines indicate the leaf water deuterium-excess, which can be used as a proxy for relative humidity (purple double arrow).

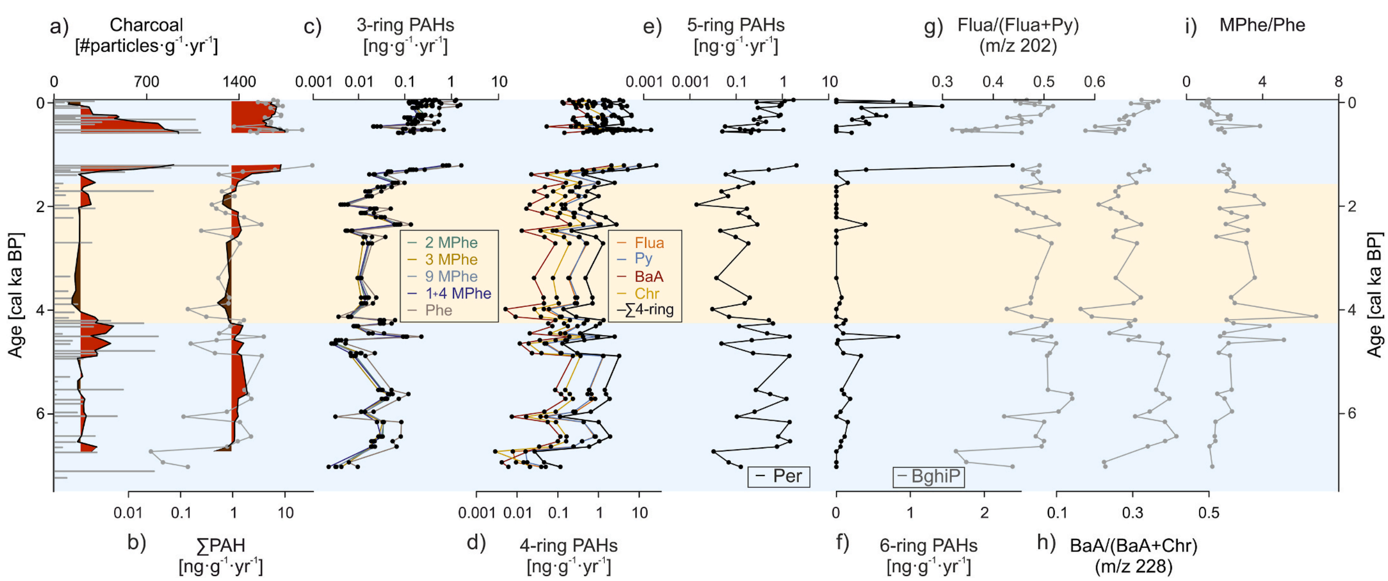

Fig. 5. a) Macro-charcoal concentrations, b) sum of 3-, 4- and 6-ring PAHs(∑PAH), c) individual concentrations of 3-ring PAHs, d) individual concentration of 4-ring PAHs and sum of 4-ring PAHs, e) 5-ring and f) 6-ring PAHs as well as diagnostic ratios of g) fluoranthene to pyrene [Flua/(Flua + Py)], h) benz(a)anthracene and chrysene [BaA/(BaA + Chr)], and i) methylphenanthrene/phenandrene (MPhe/Phe) from Vankervelsvlei. The bold line in a) and b) represents a 5-point running mean. Please note a lack of data from $1.2^{+0.2}/_{-0.1}$ to $0.6^{+0.1}/_{-0.1}$ cal ka BP due to core loss and logarithmic scale in b) to e). Blue color indicates moist conditions and high fire activity while yellow color indicates dry conditions and low fire activity.

can vary up to ~40–50‰ for $\delta^2H_{n\text{-alkane}}$ and up to ~5–8‰ for $\delta^{18}O_{sugar}$ (Gamarra et al., 2016; Lehmann et al., 2017; Sternberg, 1989). Pollen-based vegetation reconstructions at Vankervelsvlei (du Plessis et al., 2021b) and neighboring Eilandvlei (Quick et al., 2018; du Plessis et al., 2021a) indicate only minor shifts in the vegetation composition during the Mid and Late Holocene, which is underlined by minor variations in $\delta^{13}C_{n\text{-alkane}}$ and palaeontological analyses at Vankervelsvlei (Strobel et al., 2019, 2022b). The relatively stable vegetation composition at Vankervelsvlei and the surrounding wilderness area makes variations in ε_{bio}, and thus associated uncertainties in our "paleohygrometer" approach, rather unlikely. Further, climatic variations over time could bias the results of the reconstructed plant-source water, d-excess, and RH due to potential variations of the LMWL. At present, two LMWLs are available in the western and southern Cape area, i.e. from Cape Town and Mossel Bay. The slopes of the LMWL from Cape Town ($6.51 \cdot \delta^{18}O + 8.89$) and Mossel Bay ($7.70 \cdot \delta^{18}O + 12.10$) (e.g. Braun et al., 2017; Harris et al., 2010) only show minor differences. Applying the LMWL from Cape Town in the coupled-isotope approach

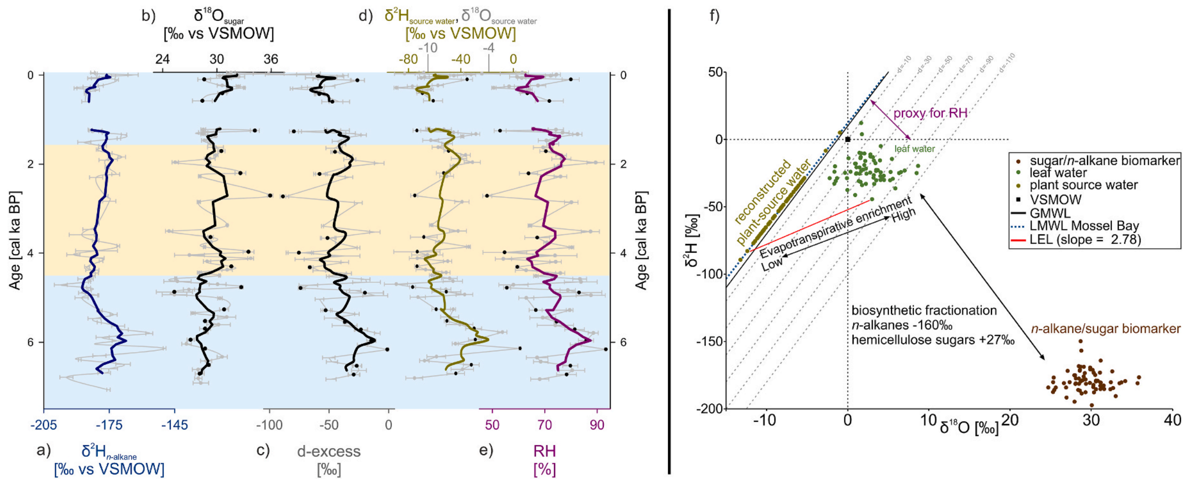

Fig. 6. a) Hydrogen isotopes ($\delta^2H_{n\text{-alkane}}$; Strobel et al., 2019, 2022a,b) from leaf wax-derived n-alkanes, b) oxygen isotopes from hemicellulose-derived sugars ($\delta^{18}O_{sugar}$), c) leaf water deuterium-excess, d) reconstructed plant-source water ($\delta^2H_{source\ water}$, $\delta^{18}O_{source\ water}$) and e) reconstructed relative humidity (RH) at Vankervelsvlei. Note that black dots in b) to e) indicate samples from an earlier study by Strobel et al. (2022a,b). The bold line in a) to e) represents a 5-point running mean. Please note a lack of data from $1.2^{+0.2}/_{-0.1}$ to $0.6^{+0.1}/_{-0.1}$ cal ka BP due to core loss. Blue color indicates moist conditions and high fire activity while yellow color indicates dry conditions and low fire activity. f) Coupled $\delta^2H_{n\text{-alkane}}$–$\delta^{18}O_{sugar}$ approach (paleohygrometer) displayed as δ^2H–$\delta^{18}O$ diagram showing the δ^2H of n-alkanes (weighted mean of C_{29} and C_{31}) and $\delta^{18}O$ of sugar (xylose) biomarkers, the reconstructed leaf and plant-source water, the global meteoric water line (GMWL, black line), and the local meteoric water line (LWML) from Mossel Bay (blue dashed line; Braun et al., 2017). The black double arrows indicate natural processes of evapotranspirative enrichment of leaf water along local evaporation lines (LEL; red line) and biosynthetic fractionation during biomarker synthesis, respectively. Grey dashed lines indicate the leaf water deuterium-excess, which can be used as a proxy for relative humidity (purple arrow).

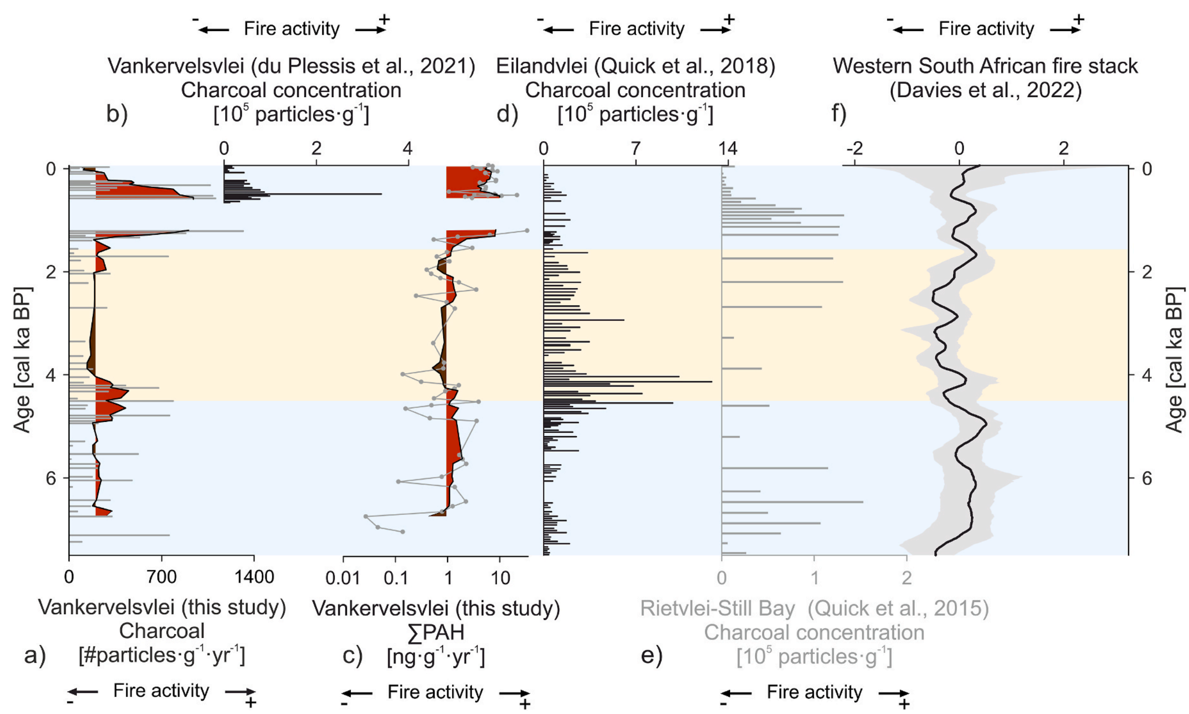

Fig. 7. Comparison of Holocene fire records from the southern Cape coast. a) Total charcoal, c) ∑PAHs from Vankervelsvlei. The bold line in a) and c) represents a 5-point running mean. For comparison, charcoal concentration from Vankervelsvlei (b) (du Plessis et al., 2021b), charcoal concentration from Eilandvlei (d) (Quick et al., 2018), and charcoal concentration Rietvlei-Still Bay (e) (Quick et al., 2015) as well as a western South African fire stack record (f) (Davies et al., 2022) are shown. Blue color indicates moist conditions and high fire activity while yellow color indicates dry conditions and low fire activity.

instead of the one from Mossel Bay would lead to changes in $\delta^{18}O_{source\ water}$ and $\delta^2H_{source\ water}$ of −0.6 to 3.3‰ (average: 1.9‰) and −1.6 to 9.3‰ (average: 5.2‰), respectively. On the one hand, a changing LMWL would therefore lead to a systematic shift, and on the other hand, this shift is within the range of the uncertainties based on error propagation of the analytical errors. Rather small variations in the slope of the LMWL over longer timescales were found in Germany (e.g. Hepp et al., 2019) supporting the application of a constant LMWL in the present study. Paleotemperature variations could lead to variations in the slope of the LEL. Over the Mid and Late Holocene, Talma and Vogel (1992) reconstructed temperature variations of 3.4 °C (15.3–18.6 °C) at Cango Cave, about 90 km northwest of Vankervelsvlei leading to changes in the slope of 0.07. Those variations lead to variations in reconstructed plant-source water of −0.2 to 0.1‰ for $\delta^{18}O_{source\ water}$ and −1.5 to 0.8‰ for δ^2H_{source}

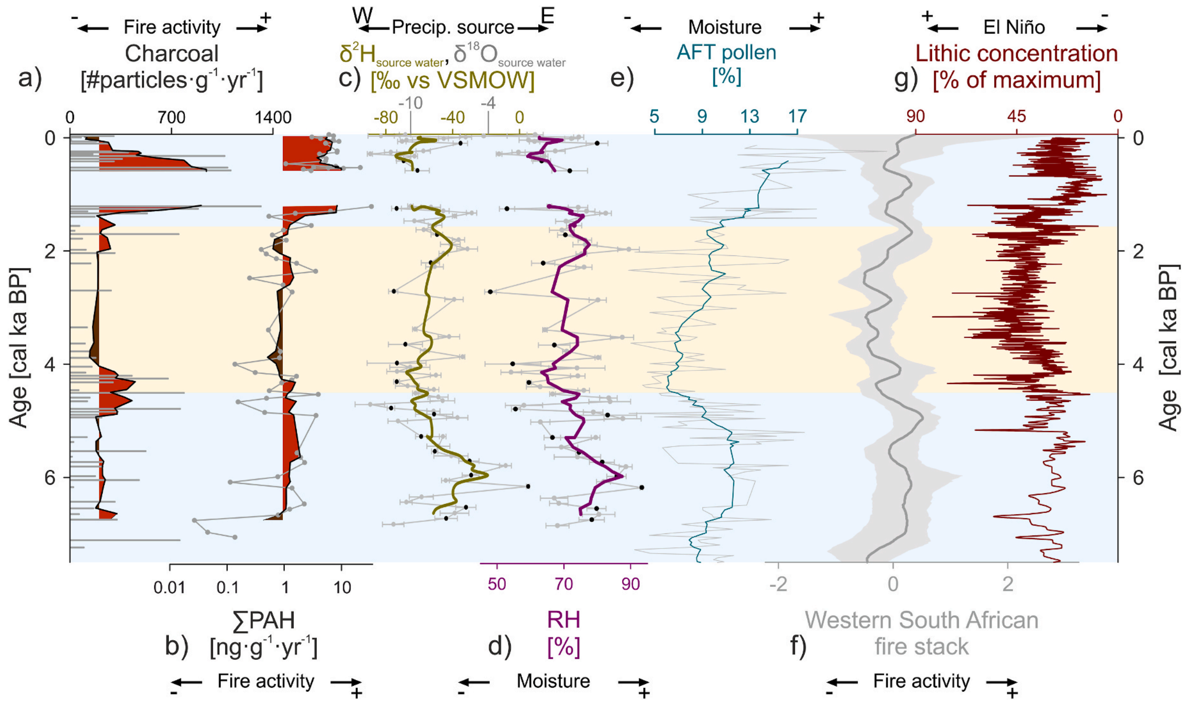

Fig. 8. Comparison of Holocene fire and climate records from Vankervelsvlei. a) Total charcoal and b) ∑PAHs as proxies for fire activity. Additionally shown are selected results from the coupled-isotope approach (paleohygrometer), i.e. c) reconstructed plant-source water ($\delta^2H_{source\ water}$, $\delta^{18}O_{source\ water)}$ as a proxy for precipitation source (W= Westerlies, E = Easterlies/local sources) and d) relative humidity (RH). The bold line in a) to d) represents a 5-point running mean. For comparison, e) Afrotemperate forest (AFT) pollen from Eilandvlei indicating moisture (Quick et al., 2018), f) a western South African fire stack record (Davies et al., 2022) and g) lithic concentration as a proxy for El Niño intensity derived from the marine sediment record SO147-106 KL recovered off Peru (Rein et al., 2005) are shown. Blue color indicates moist conditions and high fire activity while yellow color indicates dry conditions and low fire activity.

$_{water}$, which is again within the uncertainties based on error propagation of the analytical errors. Variations of the LMWL and LEL described above would also influence *d*-excess and estimated RH. However, as discussed above, those variations would be lower than the errors calculated based on the analytical uncertainties. Overall, variations of the LMWL and the LEL can lead to uncertainties in the coupled $\delta^{18}O$-δ^2H paleohygrometer approach, but those are lower than the analytical uncertainties in our study.

Previous studies demonstrate that the $\delta^2H_{n\text{-alkane}}$-$\delta^{18}O_{sugar}$-approach enables reconstruction of the isotopic composition of the plants-source water and relative humidity with a precision and accuracy of 6 ± 27‰ ($\delta^2H_{source\ water}$), 0.8 ± 3.7‰ ($\delta^{18}O_{source\ water}$) and 6 ± 17% (RH) (Strobel et al., 2020). This is comparable to climate chamber and transect studies from various environments (Hepp et al., 2020, 2021; Lemma et al., 2021; Strobel, 2022; Tuthorn et al., 2015). The coupled $\delta^2H_{n\text{-alkane}}$-$\delta^{18}O_{sugar}$-approach therefore enables a reconstruction of the isotopic composition of the plants-source water and an estimation of relative humidity.

2.6. Statistical analyses

Pearson's r-values were calculated to detect correlations between the analyzed proxies and a Student's t-test was performed to determine significant differences ($\alpha = 0.05$). To highlight trends in the data, a 5-point running mean was calculated for selected compounds. All statistical analyses were conducted using the software OriginPro 2022.

3. Results

3.1. Macro-charcoal

Macro-charcoal accumulation rates range from 7 to 1318 particles·g^{-1}·yr^{-1} with an average of 316 particles·g^{-1}·yr^{-1} (Fig. 5). Generally, macro-charcoal concentrations are high in the lower section ($7.2^{+0.2}/_{-0.2}$ to $4.0^{+0.2}/_{-0.2}$ cal ka BP), low in the middle section ($4.0^{+0.2}/_{-0.2}$ to $1.5^{+0.4}/_{-0.2}$ cal ka BP) and high in the upper section of the record ($1.5^{+0.4}/_{-0.2}$ cal ka BP until present day) (Fig. 5). However, the topmost samples show a strong decrease ($0.6^{+0.1}/_{-0.1}$ cal ka BP until present day). Exceptional peaks are present throughout the whole record with the most prominent peaks at $7.1^{+0.2}/_{-0.2}$, $6.0^{+0.2}/_{-0.2}$, $5.5^{+0.3}/_{-0.4}$, $4.8^{+0.3}/_{-0.2}$, $4.5^{+0.3}/_{-0.3}$, $4.2^{+0.3}/_{-0.2}$, $1.7^{+0.3}/_{-0.4}$, $1.3^{+0.3}/_{-0.4}$, $0.6^{+0.1}/_{-0.1}$ and $0.3^{+0.2}/_{-0.1}$ cal ka BP (Fig. 5). Macro-charcoal data is missing from $1.2^{+0.2}/_{-0.1}$ to $0.6^{+0.1}/_{-0.1}$ cal ka BP (3.9–2 m depth) because that section of the sequence was lost during coring.

3.2. Polycyclic aromatic hydrocarbons

The total PAH (∑PAH) accumulation rates varies from 0 (i.e. below the detection limit) to 34 ng•g^{-1}•yr^{-1} with an average of 3.5 ng•g^{-1}•yr^{-1} (Fig. 5). ∑PAH accumulation rates are generally high in the lower ($7.2^{+0.2}/_{-0.2}$ to $4.5^{+0.3}/_{-0.3}$ cal ka BP) and upper sections ($1.5^{+0.4}/_{-0.2}$ cal ka BP until present day) of the record, and are lower in the middle section of the record ($4.5^{+0.3}/_{-0.3}$ to $1.5^{+0.4}/_{-0.2}$ cal ka BP). PAH data are absent between $1.2^{+0.2}/_{-0.1}$ and $0.6^{+0.1}/_{-0.1}$ cal ka BP due to core loss (3.9–2 m sediment depth).

The distribution of PAHs is dominated by 4-ring PAHs, followed by 5-ring, 3-ring, and 6-ring PAHs (Fig. 5). The pattern of all compounds is variable throughout the record so we focus on the general trends (5-point running mean) of each compound in the following. The 3-ring PAH Phe ranges from 0 (i.e. below the detection limit) to 1.6 ng•g^{-1}•yr^{-1} with an average of 0.2 ng•g^{-1}•yr^{-1} and shows low values over the majority of the record, but strongly increase in the uppermost parts ($0.6^{+0.1}/_{-0.1}$ cal ka BP until present day). Its methylated isomers (2, 3, 9, 1 + 4 MPhe) follow this pattern and range from 0 (i.e. below the detection limit) to 0.9, 0.8, 0.8, and 0.6 ng•g^{-1}•yr^{-1}, respectively, with averages of 0.09, 0.08, 0.08 and 0.07 ng•g^{-1}•yr^{-1}, respectively. The sum of 4-ring PAHs (Flua, Py, BaA, Chr) ranges from 0.0 to 26.5 ng•g^{-1}•yr^{-1} with an average of 2.7 ng•g^{-1}•yr^{-1} (Fig. 5). Accumulation rates of the 4-ring PAHs are high in the bottom section ($7.2^{+0.2}/_{-0.2}$ to $4.5^{+0.3}/_{-0.3}$ cal ka BP), low in the middle section ($4.5^{+0.3}/_{-0.3}$ to $1.5^{+0.4}/_{-0.2}$ cal ka BP) and variable in the top section ($1.5^{+0.4}/_{-0.2}$ cal ka BP until present day) of the record. 5-ring PAHs (Per) range from 0.0 to 2.0 ng•g^{-1}•yr^{-1} with an average of 0.5 ng•g^{-1}•yr^{-1} and show high abundance in the lower section ($7.2^{+0.2}/_{-0.2}$ to $4.5^{+0.3}/_{-0.3}$ cal ka BP) and low accumulation rates in the middle and upper sections of the record ($4.5^{+0.3}/_{-0.3}$ cal ka BP until present day). 6-ring PAHs (BghiP) range from 0 to 2.4 ng·g^{-1} with an average of 0.2 ng·g^{-1}6-ring PAHs show a similar pattern to 4-ring PAHs and accumulation rates are high in the bottom section ($7.2^{+0.2}/_{-0.2}$ to $4.5^{+0.3}/_{-0.3}$ cal ka BP), low in the middle section ($4.5^{+0.3}/_{-0.3}$ to $1.5^{+0.4}/_{-0.2}$ cal ka BP) and variable in the top section ($1.5^{+0.4}/_{-0.2}$ cal ka BP until present day) of the record (Fig. 5).

The identified PAHs significantly correlate with each other, except for Per. The highest correlations are observed among compounds with the same number of rings, e.g. for Phe and MPhe, and BaA and Chr (Table 2).

Differences in the origin and fire regime may be deduced from PAH ratios formed within each ring-size class as the impact of environmental fractionation processes should be comparable (Yunker et al., 2002). The ratio of MPhe/Phe ranges from 0.31 to 6.81 (mean: 2.07) and shows high values from $4.5^{+0.3}/_{-0.3}$ to $1.5^{+0.4}/_{-0.2}$ cal ka BP while low values occur from $7.2^{+0.2}/_{-0.2}$ to $4.5^{+0.3}/_{-0.3}$ cal ka BP and from $1.5^{+0.4}/_{-0.2}$ cal ka BP until present day (Fig. 5). [Flua/(Flua + Py)] and [BaA/(BaA + Chr)] show a similar pattern and range from 0.32 to 0.56 (mean: 0.46), and 0.16 to 0.41 (mean 0.30), respectively (Fig. 5). Both ratios show high values from $6.6^{+0.3}/_{-0.3}$ to $4.5^{+0.3}/_{-0.3}$ cal ka BP while low values occur from $7.2^{+0.2}/_{-0.2}$ to $6.6^{+0.3}/_{-0.3}$ cal ka BP and from $4.5^{+0.3}/_{-0.3}$ to $1.5^{+0.4}/_{-0.2}$ cal ka BP. From $1.5^{+0.4}/_{-0.2}$ cal ka BP until present day, both ratios show high variability but follow a general increasing trend (Fig. 5).

3.3. *Compound-specific isotopes and paleohygrometer approach*

The oxygen isotopic composition ($\delta^{18}O_{sugar}$) of the most abundant sugar compound (xylose) in the Vankervelsvlei sediments ranges from 24.7 ± 0.4 to 35.9 ± 0.3‰ with an average of 29.6‰. There is a generally increasing trend in $\delta^{18}O_{sugar}$ over the record. Particularly, the lower section of the record ($7.2^{+0.2}/_{-0.2}$ to $4.5^{+0.3}/_{-0.3}$ cal ka BP) shows low $\delta^{18}O_{sugar}$ values compared to high $\delta^{18}O_{sugar}$ values in the middle section ($4.5^{+0.3}/_{-0.3}$ to $1.5^{+0.4}/_{-0.2}$ cal ka BP) and increasing $\delta^{18}O_{sugar}$ values in the upper section ($1.5^{+0.4}/_{-0.2}$ cal ka BP until present day) of the record. For the application of the coupled $\delta^{2}H_{n\text{-alkane}}$-$\delta^{18}O_{sugar}$-approach (paleohygrometer), $\delta^{2}H_{n\text{-alkane}}$ results from Strobel et al. (2022b) were taken into account. Results show leaf water d-excess values from −90.3 ± 13.3 to −0.5 ± 0.6‰ and have an average of −42.5‰ (Fig. 6). The lower section of the record ($7.2^{+0.2}/_{-0.2}$ to $4.5^{+0.3}/_{-0.3}$ cal ka BP) shows high leaf water d-excess values compared to low d-excess values in the middle section ($4.5^{+0.3}/_{-0.3}$ to $1.5^{+0.4}/_{-0.2}$ cal ka BP) and increasing d-excess values in the upper section ($1.5^{+0.4}/_{-0.2}$ cal ka BP until present day) of the record. Reconstructed plant-source water ranges from −89.3 ± 1.5 to 5.1 ± 0.9‰ for $\delta^{2}H$ and from −13.2 ± 1.1 to −0.9 ± 0.1‰ for $\delta^{18}O$ and show an average of −53.7 and −8.5‰, respectively. Both $\delta^{2}H_{source\ water}$ and $\delta^{18}O_{source\ water}$ show ^{2}H- and ^{18}O-enriched values in the lower section ($7.2^{+0.2}/_{-0.2}$ to $4.5^{+0.3}/_{-0.3}$ cal ka BP), ^{2}H- and ^{18}O-depleted values in the middle section ($4.5^{+0.3}/_{-0.3}$ to $1.5^{+0.4}/_{-0.2}$ cal ka BP) and increasing ^{2}H- and ^{18}O-enriched values in the upper section ($1.5^{+0.4}/_{-0.2}$ cal ka BP until present day) of the record. Reconstructed RH ranges from 45.9 ± 7 to 93.4 ± 0.4% and shows an average of 71.2% (Fig. 6). Reconstructed RH shows high values in the lower section ($7.2^{+0.2}/_{-0.2}$ to $4.5^{+0.3}/_{-0.3}$ cal ka BP), low values in the middle section ($4.5^{+0.3}/_{-0.3}$ to $1.5^{+0.4}/_{-0.2}$ cal ka BP) and variable but slightly increasing RH-values in the upper section ($1.5^{+0.4}/_{-0.2}$ cal ka BP until present day) of the record (Fig. 6).

Table 2
Pearson's correlations between the relative concentrations of the 8 components of polycyclic aromatic hydrocarbons (PAHs) used in the analysis. Bold values indicate significant correlations at the 0.05 level. Italic numbers indicate the number of aromatic rings of each PAH.

PAHs	Phe *(3)*	MPhe *(3)*	Flua *(4)*	Py *(4)*	BaA *(4)*	Chr *(4)*	Per *(5)*	BghiP *(6)*
Phe *(3)*	1							
MPhe *(3)*	**0.91**	1						
Flua *(4)*	**0.51**	**0.74**	1					
Py *(4)*	**0.51**	**0.75**	**0.97**	1				
BaA *(4)*	**0.54**	**0.77**	**0.95**	**0.96**	1			
Chr *(4)*	**0.48**	**0.72**	**0.86**	**0.92**	**0.94**	1		
Per *(5)*	0.18	0.20	**0.40**	**0.32**	**0.33**	0.14	1	
BghiP *(6)*	**0.58**	**0.57**	**0.38**	**0.34**	**0.38**	**0.29**	**0.31**	1

4. Discussion

4.1. *Paleofire dynamics along South Africa's southern Cape coast*

PAH fingerprints may be biased by transport and degradation, which shall be discussed before stepping into the reconstruction of fire history. Vankervelsvlei sediments show high organic matter preservation indicated by high TOC contents and low variability in molar C/N ratio, $\delta^{13}C_{TOC}$ and $\delta^{15}N$ indicating low peat degradation (Meyers, 2003; Strobel et al., 2022b). The PAH composition and pattern could, however, potentially be biased by degradation or differential transport (Lima et al., 2005; Stogiannidis and Laane, 2015). The dominance of 4-ring over 5 and 6-ring PAHs makes degradation effects rather unlikely (Lima et al., 2005). For further details regarding degradation types impacting PAHs in sediments, the reader is referred, for example, to the review by Lima et al. (2005).

The ranges of Methylphenanthrene to Phenanthrene (MPhe/Phe), Fluoranthene to Pyrene [Flua/(Flua + Py)], and Benz(a)anthracene to Chrysene [BaA/(BaA + Chr)] throughout our record indicate a mixed origin of the respective PAH compounds from pyrogenic and petrogenic sources (Fig. 5) (e.g. Stogiannidis and Laane, 2015; Yunker et al., 2002; Zhang et al., 2008). However, the prevailing geology in the studied area consists of dunes, sandstones, and quartzites (Johnson et al., 2006) making petrogenic PAH sources highly improbable up until modern anthropogenic influence (e.g. Garrigues et al., 1995; Kirsten et al., 2023; Zhang et al., 2008). Alternatively, some studies suggest that diagnostic PAH ratios of [Flua/(Flua + Py)] and [BaA/(BaA + Chr)] can be used to differentiate fuel types (softwood and shrubs vs. hardwood) but differences are often statistically insignificant limiting the applicability of both ratios for differentiating softwood and shrubs versus hardwood combustion residuals (Fine et al., 2001, 2002; Gonçalves et al., 2010; Oros et al., 2006; Oros and Simoneit, 2001a, 2001b; Rogge et al., 1998; Vicente et al., 2016; Wang et al., 2009). Other PAHs that could decipher changes in the fuels of fire at Vankervelsvlei more clearly, i.e. dimethylated phenanthrenes and retene (m/z 234) (e.g. Benner et al., 1995; Kappenberg et al., 2019; Karp et al., 2020; Miller et al., 2017), are unfortunately absent in our samples and/or were not targeted during analyses.

Although we cannot fully exclude the aforementioned biases in our PAH record the good agreement with our macro-charcoal record likely indicates that at least the majority of PAHs are of pyrogenic origin at Vankervelsvlei. Therefore, we will discuss variations in ∑PAHs in terms of fire activity at Vankervelsvlei.

High macro-charcoal and $\sum$PAH accumulation rates indicate high local fire activity at Vankervelsvlei from $7.2^{+0.2}/_{-0.2}$ to $4.5^{+0.3}/_{-0.3}$ cal ka BP. In contrast, low macro-charcoal and low $\sum$PAH accumulation rates indicate less pronounced local fire activity from $4.5^{+0.3}/_{-0.3}$ to $1.5^{+0.4}/_{-0.2}$ cal ka BP. From $1.5^{+0.4}/_{-0.2}$ cal ka BP until present, macro-charcoal and $\sum$PAH accumulation rates show high fire activity. However, from $0.6^{+0.1}/_{-0.1}$ cal ka BP until present day charcoal and $\sum$PAH accumulation rates show divergent patterns. While macro-charcoal accumulation rates decrease, $\sum$PAH accumulation rates are still high. Decreasing charcoal accumulation rates during the past have also been observed in a previous study at Vankervelsvlei focusing on the past $0.6^{+0.1}/_{-0.1}$ cal ka BP (du Plessis et al., 2021b) (Fig. 7).

A charcoal record from Rietvlei-Still Bay (~130 km SW from Vankervelsvlei) (Quick et al., 2015) and a recently compiled charcoal-based fire stack record for western South Africa including the southern Cape, (Davies et al., 2022) resemble fire activity at Vankervelsvlei (Fig. 7). Like Vankervelsvlei, both records show high fire activity in the early Mid Holocene (Rietvlei-Still Bay: 7.5 to 5.8 cal ka BP; western fire stack: 7.2 to 4.5 cal ka BP). Conversely, a charcoal record from Eilandvlei (~25 km west of Vankervelsvlei) shows low fire activity from 7.5 to 4.5 cal ka BP but pronounced fire activity from 4.5 to 4.0 cal ka BP (Quick et al., 2018) that corresponds with high charcoal-derived fire activity at Vankervelsvlei from $4.5^{+0.3}/_{-0.3}$ to $4.2^{+0.3}/_{-0.2}$ cal ka BP. This is followed by low fire activity at Vankervelsvlei being in line with reduced fire activity at Rietvlei-Still Bay (5.8–3.3 cal ka BP), Eilandvlei (4.0 cal ka BP until present day) and in the western fire stack (~4.5–~2.0 cal ka BP). In the last two millennia, high fire activity at Vankervelsvlei is consistent with the western fire stack (Davies et al., 2022) (Fig. 7), but contradicts charcoal-based records from Bo Langvlei (du Plessis et al., 2020), Rietvlei-Still Bay (Quick et al., 2015) and Eilandvlei (du Plessis et al., 2021a; Quick et al., 2018).

On the one hand, previous charcoal studies have demonstrated long-term changes in fire activity on the southern Cape coast with evidence from Eilandvlei (du Plessis et al., 2021a; Quick et al., 2018), Bo Langvlei (du Plessis et al., 2020), Vankervelsvlei (du Plessis et al., 2021b; Quick et al., 2016) and Rietvlei-Still Bay (Quick et al., 2015), but most of these records either refer to specific periods, have low temporal resolution and/or show limited chronological control. On the other hand, diverging trends of pyrogenic records like charcoal and PAHs have previously been observed and attributed to changes in land-use and anthropogenic fires (e.g. Bandowe et al., 2014; Hanke et al., 2016; Lehndorff et al., 2015; Vachula et al., 2022). While natural fires might have been controlled or limited to a certain degree, as reflected in the charcoal record, anthropogenic fires could have increased with the expanding population, possibly explaining the increasing $\sum$PAHs (Bandowe et al., 2014; Chimuka et al., 2016; Lehndorff et al., 2015). In our Vankervelsvlei record, it is noticeable that 3-ring PAHs are generally low during the major parts of the record but distinctly contribute to increasing $\sum$PAH from $0.6^{+0.1}/_{-0.1}$ cal ka BP until present day (Fig. 5). 3-ring PAHs are more volatile compounds compared to the other PAH compounds (Johnsen et al., 2005; Kim et al., 2011) analyzed in this study. Warm and dry summer conditions from $4.5^{+0.3}/_{-0.3}$ to $1.5^{+0.4}/_{-0.2}$ cal ka BP might lead to re-volatilisation of the previously accumulated 3-ring PAHs from the sediments which possibly explains the low concentrations in parts of the record. However, more likely, the increasing 3-ring PAHs indicate a distinct contribution of pyrogenic components during the past $0.6^{+0.1}/_{-0.1}$ years differing from the natural fires dominating the major parts of the Vankervelsvlei record. The increasing number of controlled low-temperature wildfires and anthropogenic fire, including wood combustion for food production, could be a potential cause of the increasing 3-ring PAHs (Chimuka et al., 2016; Deacon et al., 1984; Lehndorff et al., 2015). This is in line with the increasing population and anthropogenic fire activity in southern Africa during this time (e.g. Davies et al., 2022; Deacon et al., 1984).

Although looking at trends (5-point running mean), we note that differences in the applied methodological approach (e.g. sampling resolution and distance, charcoal size classes, units [concentrations, counts] in which charcoal is displayed), individual age control, and the prevailing site-specific environmental setting affecting production, transport, and deposition of combustion-derived particles (e.g. source area, vegetation characteristics, hydrological conditions within the watershed, sedimentological processes) all potentially contribute to differences in the records used for comparison (e.g. Hennebelle et al., 2020; Vachula et al., 2022; Vachula and Richter, 2018; Vachula et al., 2018). Additionally, discontinuous sampling and integration of several fire events in one sample, i.e. 1 cm samples integrates up to multiple decades in some studies, all of which might explain differences and/or the absences of individual peaks. Moreover, existing charcoal records from estuarine environments (e.g. Eilandvlei, Rietvlei-Still Bay) might be biased due to marine water intrusions and potential changes in water level, morphology, as well as sediment mixing and deposition (du Plessis et al., 2020; du Plessis et al., 2021a; Quick et al., 2015; Quick et al., 2018). Although fire records from Eilandvlei show a partly divergent pattern, records from Vankervelsvlei and Rietvlei-Still Bay, and a fire stack record for western South Africa indicate a coherent fire pattern along South Africa's southern Cape coast including high fire activity from 7.2 to 4.5 cal ka BP and low fire activity from 4.5 to 2.0 cal ka BP. Subsequent contradictions might be explained by increasing anthropogenic fire activity (ignition and suppression) along the western and southern South African coast.

4.2. Paleoclimatic controls on fire dynamic along the southern Cape coast

Past changes in the atmospheric source and seasonality of precipitation as well as local relative humidity at Vankervelsvlei and along the southern Cape coast have previously been discussed by Strobel et al. (2022b) including the application of the coupled $\delta^2H_{n\text{-alkane}} - \delta^{18}O_{sugar}$ (paleohygrometer) approach. However, the temporal resolution of this approach has been limited so far. In this study, we distinctly increased the temporal resolution of $\delta^{18}O_{sugar}$ complementing previous high-resolution $\delta^2H_{n\text{-alkane}}$ results (Strobel et al., 2022b). This allows for the calculation of the plants-source water ($\delta^2H_{source\ water,}$ $\delta^{18}O_{source\ water}$) referring to the atmospheric source and seasonality of precipitation, and the local RH in high temporal resolution, which ultimately strengthens the significance of the paleohydrological record from Vankervelsvlei.

From $7.2^{+0.2}/_{-0.2}$ to $4.5^{+0.3}/_{-0.3}$ cal ka BP, high RH values coincide with more positive values of plant-source water indicating distinct precipitation contributions of both Westerly-derived winter precipitation and Easterly- and/or locally-derived summer precipitation and thus moist conditions year-round (Fig. 8). $\sum$PAH, originating from the identical samples as the aforementioned climatic proxies, and macro-charcoal concentrations indicate high fire activity at that period ($7.2^{+0.2}/_{-0.2}$ to $4.5^{+0.3}/_{-0.3}$ cal ka BP) (Fig. 8).

From $4.5^{+0.3}/_{-0.3}$ to $1.5^{+0.4}/_{-0.2}$ cal ka BP, low RH values coincide with more negative values of plant-source water indicating the dominance of Westerly-derived winter precipitation, but suggesting a weakening of Easterly- and/or locally-derived summer precipitation. Overall drier conditions occurred at Vankervelsvlei and along the southern Cape coast including a shift towards a winter rainfall regime during this period (Strobel et al., 2022b) (Fig. 8). During these drier conditions $\sum$PAH and macro-charcoal concentrations suggest low fire activity from $4.5^{+0.3}/_{-0.3}$ to $1.5^{+0.4}/_{-0.2}$ cal ka BP (Fig. 8).

From $1.5^{+0.4}/_{-0.2}$ cal ka BP until present day, a shift towards a year-round rainfall regime at Vankervelsvlei and along the southern Cape coast is indicated by increased RH values coinciding with more positive values of plant-source water (Fig. 8). Although increasing anthropogenic impact on fire dynamics at Vankervelsvlei, i.e. human-made and more controlled wildfires, is suggested based on $\sum$PAH increase while macro-charcoal concentrations decrease from $1.5^{+0.4}/_{-0.2}$ cal ka BP until present day (Fig. 8).

This climatic pattern at Vankervelsvlei has previously been described by Strobel et al. (2022b). The pattern of RH and plant-source water

($\delta^2H_{source\ water}$ and $\delta^{18}O_{source\ water}$) at Vankervelsvlei resembles the abundance of Afrotemperate forest (AFT) pollen at neighboring Eilandvlei (Fig. 8). The latter is located ~25 km to the west of Vankervelsvlei (Fig. 2). The AFT pollen signal is an indicator for moisture availability at the site and the surrounding Wilderness area, including Vankervelsvlei (Quick et al., 2018), being in line with other moisture indicators from Eilandvlei (e.g. Wündsch et al., 2018). The relationship between RH, plant-source water, and AFT pollen suggests a consistent enhancement in the moisture signal in the Wilderness area during the Holocene implying that moist conditions are associated with increased precipitation contributed during summer (Easterlies) and/or from local sources. Conversely, dry conditions are associated with less precipitation contribution during summer (Easterlies and/or from local sources). This is in line with results from paleoclimatic records located along the southern Cape coast derived using methods from disciplines such as palynology, palaeontology as well as organic, inorganic, and stable isotope geochemistry (e.g. Hahn et al., 2017; Kirsten et al., 2018; Quick et al., 2015; Quick et al., 2018; Strobel et al., 2021; Wündsch et al., 2018; Wündsch et al., 2016) providing a coherent moisture evolution and atmospheric precipitation source signal along South Africa's southern Cape coast.

Fire dynamics at Vankervelsvlei and along the southern Cape coast likely changed in response to the shifting regional climate, i.e. precipitation seasonality and local relative humidity, during the Holocene. In this context, previous studies have shown that local moisture availability and temperature largely drive fuel productivity and fuel moisture which in turn control fire incidence, frequency, seasonality, and intensity (Daniau et al., 2012; Jolly et al., 2015; Kraaij et al., 2022; Kraaij and van Wilgen, 2014; Msweli et al., 2020). While this study provides robust precipitation source and local moisture availability records for the southern Cape coast, the region still lacks continuous Holocene temperature reconstructions with sufficient temporal resolution and chronological control (e.g. Talma and Vogel, 1992). As temperature reconstructions become available (e.g. Loehle, 2007), a more comprehensive understanding of paleoclimate and environmental responses will emerge. However, fire regimes with high fire activity and efficient fuel conditions have been linked to periods of increased moisture (i.e. $7.2^{+0.2}/_{-0.2}$ to $4.5^{+0.3}/_{-0.3}$ cal ka BP) as a result of the intensification of both the Easterly- and locally-derived summer precipitation as well as Westerly-derived winter precipitation (Fig. 8). Conversely, reconstructed fire regimes suggest fire decreases when fuel availability is reduced during protracted drought periods ($4.5^{+0.3}/_{-0.3}$ to $1.5^{+0.4}/_{-0.2}$ cal ka BP) driven by an overall reduction in total precipitation from a weakening of the Easterlies and local moisture sources during summer and a more persistent winter rainfall regime (Fig. 8).

The pattern of our precipitation source and local moisture availability record resembles the Western South African fire stack (Davies et al., 2022) (Fig. 8) showing high fire activity during phases of increased fuel availability due to low precipitation seasonality (year-round rainfall regime) and high local relative humidity. Conversely, low fire activity occurs during phases of decreased fuel availability as a result of high precipitation seasonality (winter rainfall regime) and low local relative humidity (Fig. 8). This highlights that our reconstructed climatic pattern drives fuel availability at Vankervelsvlei and along the southern Cape coast, and potentially extends further west. However, for evaluating the longitudinal extent of the climatic pattern and fire activity, there is a need for further records providing high temporal resolution and precise chronological control in the winter rainfall zone of South Africa.

Our precipitation source and relative humidity records are also comparable to the intensity of El Niño Southern Oscillation (ENSO) highlighting the influence of the latter on South Africa's regional climate (Fig. 8). Generally, low precipitation seasonality (year-round precipitation regime) and high local relative humidity are accompanied by low ENSO intensity (i.e. $7.2^{+0.2}/_{-0.2}$ to $4.5^{+0.3}/_{-0.3}$ cal ka BP and $1.5^{+0.4}/_{-0.2}$ cal ka BP until present day). Conversely, high precipitation seasonality (winter rainfall regime) and low local relative humidity are accompanied by high ENSO intensity (Fig. 8). This is perfectly in line with recent observations of prolonged drought periods in South Africa during summer, which has been attributed to the absence of Easterly-derived summer precipitation along the southern Cape coast due to ENSO events (Blamey et al., 2018; Engelbrecht and Landman, 2016; Favre et al., 2013; Ratnam et al., 2014; Weldon and Reason, 2014). Furthermore, ENSO events have been attributed to an increase in fire probability in this area (Burton et al., 2020; Duane et al., 2021). However, our fire activity records (macro-charcoal and $\sum$PAH concentrations) from Vankervelsvlei and ENSO intensity (Rein et al., 2004, 2005) (Fig. 8) show an opposed pattern indicating high (low) fire activity along South Africa's southern Cape coast contemporaneous with decreased (increased) ENSO intensity (Fig. 8). This likely indicates that fire activity along the southern Cape coast prominently depends on fuel availability, which is related to long-term climatic trends. On the other hand, high biomass availability during generally humid periods (i.e. $7.2^{+0.2}/_{-0.2}$ to $4.5^{+0.3}/_{-0.3}$ cal ka BP and $1.5^{+0.4}/_{-0.2}$ cal ka BP until present day) provides potential for extensive burning, possibly induced by single or low intense ENSO events. In turn, during generally dry conditions (i.e. $4.5^{+0.3}/_{-0.3}$ to $1.5^{+0.4}/_{-0.2}$ cal ka BP) biomass availability is limited and fire activity is low, although intense ENSO events provide the potential for frequent fire weather at Vankervelsvlei and along South Africa's southern Cape coast (Fig. 8).

Drought-adaptive, fire-resistant and/or dependent ecosystems (such as Fynbos) can survive along the southern Cape coast, benefitting the region's biodiversity. To protect biodiversity in the face of future climate change and its projected impacts on fire frequency and ENSO intensity, southern Cape coast ecosystems must be adaptive, resilient, and resistant against extreme events (precipitation, drought, and fires). Rapid transitions between contrasting periods of extreme conditions provide the ideal scenario for fuel load increase, resulting in intense fires. If ecosystems are unable to adapt accordingly, this can lead to stress and/or mortality (Milton et al., 2022).

5. Conclusion

The southern Cape coast of South Africa experienced variable fire activity associated with paleoclimatic and paleoecological changes during the Holocene. Our multi-proxy record from Vankervelsvlei provides new insights into fire and climatic dynamics at South Africa's southern Cape coast during the Holocene.

Our study highlights that fire dynamics at Vankervelsvlei and along the southern Cape coast likely changed in response to the shifting regional climate during the Holocene. From $7.2^{+0.2}/_{-0.2}$ to $4.5^{+0.3}/_{-0.3}$ cal ka BP, high macro-charcoal and $\sum$PAH accumulation rates indicate high fire activity at Vankervelsvlei promoted by generally moist conditions and a year-round rainfall regime due to the contributions of both Westerly-derived winter precipitation and Easterly- and locally-derived summer precipitation. From $4.5^{+0.3}/_{-0.3}$ to $1.5^{+0.4}/_{-0.2}$ cal ka BP, lower macro-charcoal and $\sum$PAH accumulation rates indicate lower fire activity. Contemporaneously, rather dry conditions occurred due to the presence of Westerly-derived winter precipitation but a decrease of Easterly- and locally-derived summer precipitation leading to a shift toward a winter rainfall regime. During the past $1.5^{+0.4}/_{-0.2}$ years, moisture has been variable but generally increasing due to increasing contributions of both the Westerly-derived winter precipitation and the Easterly- and locally-derived summer precipitation, leading to the presence of a year-round rainfall regime along the southern Cape coast. As a result, macro-charcoal and $\sum$PAH accumulation rates are generally high from $1.5^{+0.4}/_{-0.2}$ cal ka BP until present day while charcoal accumulation rates show a decreasing trend from $0.6^{+0.1}/_{-0.1}$ cal ka BP until present probably due to the impact of anthropogenic activities.

Results of our record are generally in line with previous investigations at Vankervelsvlei and closely located paleopyrogenic and paleoclimatic records along the southern Cape coast. Moreover, our record from Vankervelsvlei is consistent with a recently developed fire stack record from western South Africa. In this context, El Niño impacts the regional precipitation regime along the southern Cape coast. During intense El Niño, summer precipitation is dramatically low increasing the potential for wildfires. For example, during generally moist periods (e.g. $7.2^{+0.2}/_{-0.2}$ to $4.5^{+0.3}/_{-0.3}$ cal ka BP and $1.5^{+0.4}/_{-0.2}$ to present day) there is a high biomass availability but El Niño-induced drought during summer likely leads to high potential for destructive fires along the southern Cape coast. El Niño is predicted to increase in the future providing potential for increased fire activity along the southern Cape coast. This will have relevance for future management of fire regimes. For a more comprehensive understanding of past fire, vegetation, and climate relations, there is a need for future studies investigating well-established and innovative pyrogenic (e.g. macro-charcoal, PAHs, etc.), palynological and direct hydrological proxies, i.e. $\delta^{18}O_{sugar}$ and $\delta^{2}H_{n\text{-alkane}}$, in identical samples from the same site allowing more robust reconstructions.

In order to get a better understanding of the interplay of various fire proxies, a comparison with known fire events is needed. This will contribute to a better understanding of which fire characteristics are reflected by each proxy, such as fire frequency, intensity, proximity, fuel type, or area burnt. Moreover, combustion residuals of different vegetation types exhibit a distinct pyrogenic signature, requiring further investigation into the prevalent plant species on the southern Cape coast and their specific fingerprints in the combustion-related production of pyrogenic compounds. This, in turn, will contribute to a better assessment of future regional fire dynamics in the context of ongoing climate change, as well as improved conservation and management of the unique biodiversity and human habitat protection on the southern Cape coast of South Africa.

Funding

This study was funded by the German Research Foundation (DFG) (HA 5089/11–1; 800ZE 860/6–1).

CRediT authorship contribution statement

Paul Strobel: Conceptualization, Formal analysis, Funding acquisition, Investigation, Writing - original draft, Writing - review & editing. **Theresa Henning:** Investigation, Writing - review & editing. **Marcel Bliedtner:** Investigation, Writing - review & editing. **Stella G. Mosher:** Investigation, Writing - review & editing. **Humay Rahimova:** Investigation, Writing - review & editing. **Torsten Haberzettl:** Funding acquisition, Access to sediments, Writing - review & editing. **Kelly L. Kirsten:** Writing - review & editing. **Eva Lehndorff:** Writing - review & editing. **Mitchell J. Power:** Writing - review & editing. **Michael Zech:** Writing - review & editing. **Roland Zech:** Funding acquisition, Writing - review & editing.

Declaration of competing interest

The authors declare that they have no known competing financial interests or personal relationships that could have appeared to influence the work reported in this paper.

Data availability

The datasets analyzed for this study is available at Pangaea: https://doi.org/10.1594/PANGAEA.956477. Previously published data by Strobel et al. (2022a) used for comparison is also available at Pangaea (https://doi.pangaea.de/10.1594/PANGAEA.940148)

Acknowledgments

The authors would like to thank three anonymous reviewers for their very valuable comments and suggestions that improved this manuscript. This study was funded by the German Research Foundation (DFG) (HA 5089/11–1; ZE 860/6–1). The authors would like to thank the participants of the 2016 Vankervelsvlei expedition for help with core recovery. The authors thank Olivia Shulte for supporting sample preparation for macro-charcoal analyses and Lucas Bittner for supporting $\delta^{18}O_{sugar}$ analyses.

References

Amelung, W., Cheshire, M.V., Guggenberger, G., 1996. Determination of neutral and acidic sugars in soil by capillary gas-liquid chromatography after trifluoroacetic acid hydrolysis. Soil Biol. Biochem. 28, 1631–1639.

Andela, N., Morton, D.C., Giglio, L., Randerson, J.T., 2019. Global Fire Atlas with Characteristics of Individual Fires, 2003-2016. ORNL Distributed Active Archive Center.

Archibald, S., Roy, D.P., Van Wilgen, B.W., Scholes, R.J., 2009. What limits fire? An examination of drivers of burnt area in Southern Africa. Global Change Biol. 15, 613–630.

Argiriadis, E., Battistel, D., McWethy, D.B., Vecchiato, M., Kirchgeorg, T., Kehrwald, N. M., Whitlock, C., Wilmshurst, J.M., Barbante, C., 2018. Lake sediment fecal and biomass burning biomarkers provide direct evidence for prehistoric human-lit fires in New Zealand. Sci. Rep. 8, 12113.

Bandowe, B.A.M., Srinivasan, P., Seelge, M., Sirocko, F., Wilcke, W., 2014. A 2600-year record of past polycyclic aromatic hydrocarbons (PAHs) deposition at Holzmaar (Eifel, Germany). Palaeogeogr. Palaeoclimatol. Palaeoecol. 401, 111–121.

Bateman, M.D., Carr, A.S., Dunajko, A.C., Holmes, P.J., Roberts, D.L., McLaren, S.J., Bryant, R.G., Marker, M.E., Murray-Wallace, C.V., 2011. The evolution of coastal barrier systems: a case study of the Middle-Late Pleistocene Wilderness barriers, South Africa. Quat. Sci. Rev. 30, 63–81.

Battistel, D., Argiriadis, E., Kehrwald, N., Spigariol, M., Russell, J.M., Barbante, C., 2016. Fire and human record at lake victoria, east Africa, during the early iron age: did humans or climate cause massive ecosystem changes? Holocene 27, 997–1007.

Benner, B.A., Wise, S.A., Currie, L.A., Klouda, G.A., Klinedinst, D.B., Zweidinger, R.B., Stevens, R.K., Lewis, C.W., 1995. Distinguishing the contributions of residential wood combustion and mobile source emissions using relative concentrations of dimethylphenanthrene isomers. Environ. Sci. Technol. 29, 2382–2389.

Blaauw, M., Christen, J.A., 2011. Flexible paleoclimate age-depth models using an autoregressive gamma process. Bayesian Analysis 6, 457–474.

Blamey, R.C., Kolusu, S.R., Mahlalela, P., Todd, M.C., Reason, C.J.C., 2018. The role of regional circulation features in regulating El Niño climate impacts over southern Africa: a comparison of the 2015/2016 drought with previous events. Int. J. Climatol. 38, 4276–4295.

Bläsing, M., Amelung, W., Schwark, L., Lehndorff, E., 2017. Inland navigation: PAH inventories in soil and vegetation after EU fuel regulation 2009/30/EC. Sci. Total Environ. 584–585, 19–28.

Bläsing, M., Kistler, M., Lehndorff, E., 2016. Emission fingerprint of inland navigation vessels compared with road traffic, domestic heating and ocean going vessels. Org. Geochem. 99, 1–9.

Bond, W.J., Midgley, G.F., Woodward, F.I., 2003. What controls South African vegetation – climate or fire? South Afr. J. Bot. 69, 79–91.

Bowen, G.J., 2022. The Online Isotopes in Precipitation Calculator version 3.1. URL: http://www.waterisotopes.org.

Bowen, G.J., Wassenaar, L.I., Hobson, K.A., 2005. Global application of stable hydrogen and oxygen isotopes to wildlife forensics. Oecologia 143, 337–348.

Braun, K., Bar-Matthews, M., Ayalon, A., Zilberman, T., Matthews, A., 2017. Rainfall isotopic variability at the intersection between winter and summer rainfall regimes in coastal South Africa (Mossel Bay, Western Cape Province). S. Afr. J. Geol. 120, 323–340.

Burton, C., Betts, R.A., Jones, C.D., Feldpausch, T.R., Cardoso, M., Anderson, L.O., 2020. El Niño driven changes in global fire 2015/16. Front. Earth Sci. 8, 1–12.

Callegaro, A., Battistel, D., Kehrwald, N.M., Matsubara Pereira, F., Kirchgeorg, T., Villoslada Hidalgo, M.D.C., Bird, B.W., Barbante, C., 2018. Fire, vegetation, and Holocene climate in a southeastern Tibetan lake: a multi-biomarker reconstruction from Paru Co. Clim. Past 14, 1543–1563.

Cernusak, L.A., Barbeta, A., Bush, R.T., Eichstaedt, R., Ferrio, J.P., Flanagan, L.B., Gessler, A., Martín-Gómez, P., Hirl, R.T., Kahmen, A., Keitel, C., Lai, C.-T., Munksgaard, N.C., Nelson, D.B., Ogée, J., Roden, J.S., Schnyder, H., Voelker, S.L., Wang, L., Stuart-Williams, H., Wingate, L., Yu, W., Zhao, L., Cuntz, M., 2022. Do 2H and 18O in leaf water reflect environmental drivers differently? New Phytol. 235, 41–51.

Cernusak, L.A., Wong, S.C., Farquhar, G.D., 2003. Oxygen isotope composition of phloem sap in relation to leaf water in Ricinus communis. Funct. Plant Biol. 30, 1059–1070.

Chase, B.M., Meadows, M.E., 2007. Late Quaternary dynamics of southern Africa's winter rainfall zone. Earth Sci. Rev. 84, 103–138.

Chimuka, L., Sibiya, P., Amdany, R., Cukrowska, E., Forbes, P.B.C., 2016. Status of PAHs in environmental compartments of South Africa: a country report. Polycycl. Aromat. Comp. 36, 376–394.

Conedera, M., Tinner, W., Neff, C., Meurer, M., Dickens, A.F., Krebs, P., 2009. Reconstructing past fire regimes: methods, applications, and relevance to fire management and conservation. Quat. Sci. Rev. 28, 555–576.

Daniau, A.L., Bartlein, P.J., Harrison, S.P., Prentice, I.C., Brewer, S., Friedlingstein, P., Harrison-Prentice, T.I., Inoue, J., Izumi, K., Marlon, J.R., Mooney, S., Power, M.J., Stevenson, J., Tinner, W., Andrič, M., Atanassova, J., Behling, H., Black, M., Blarquez, O., Brown, K.J., Carcaillet, C., Colhoun, E.A., Colombaroli, D., Davis, B.A. S., D'Costa, D., Dodson, J., Dupont, L., Eshetu, Z., Gavin, D.G., Genries, A., Haberle, S., Hallett, D.J., Hope, G., Horn, S.P., Kassa, T.G., Katamura, F., Kennedy, L. M., Kershaw, P., Krivonogov, S., Long, C., Magri, D., Marinova, E., McKenzie, G.M., Moreno, P.I., Moss, P., Neumann, F.H., Norström, E., Paitre, C., Rius, D., Roberts, N., Robinson, G.S., Sasaki, N., Scott, L., Takahara, H., Terwilliger, V., Thevenon, F., Turner, R., Valsecchi, V.G., Vannière, B., Walsh, M., Williams, N., Zhang, Y., 2012. Predictability of biomass burning in response to climate changes. Global Biogeochem. Cycles 26, 1–12.

Dansgaard, W., 1964. Stable isotopes in precipitation. Tellus 16, 436–468.

Davies, B., Power, M.J., Braun, D.R., Douglass, M.J., Mosher, S.G., Quick, L.J., Esteban, I., Sealy, J., Parkington, J., Faith, J.T., 2022. Fire and human management of late Holocene ecosystems in southern Africa. Quat. Sci. Rev. 289, 107600.

Deacon, H.J., Deacon, J., Scholtz, A., Thackeray, J.F., Brink, J.S., 1984. Correlation of palaeoenvironmental data from the late pleistocene and Holocene deposits at boomplaas Cave, southern Cape. In: Vogel, J.C. (Ed.), Late Cainozoic Palaeoclimates of the Southern Hemisphere. Balkema, Rotterdam, pp. 339–360.

Denis, E.H., Toney, J.L., Tarozo, R., Scott Anderson, R., Roach, L.D., Huang, Y., 2012. Polycyclic aromatic hydrocarbons (PAHs) in lake sediments record historic fire events: validation using HPLC-fluorescence detection. Org. Geochem. 45, 7–17.

du Plessis, N., Chase, B.M., Quick, L.J., Haberzettl, T., Kasper, T., Meadows, M.E., 2020. Vegetation and climate change during the medieval climate anomaly and the little ice age on the southern Cape coast of South Africa: pollen evidence from Bo Langvlei. Holocene 30, 1716–1727.

du Plessis, N., Chase, B.M., Quick, L.J., Meadows, M.E., 2021a. A Late Holocene pollen and microcharcoal record from Eilandvlei, southern Cape coast, South Africa. In: Runge, J., Gosling, W.D., Lézine, A.-M., Scott, L. (Eds.), Quaternary Vegetation Dynamics – the African Pollen Database. CRC Press, London, pp. 293–300.

du Plessis, N., Chase, B.M., Quick, L.J., Strobel, P., Haberzettl, T., Meadows, M.E., 2021b. A c. 650 year pollen and microcharcoal record from Vankervelsvlei, South Africa. In: Runge, J., Gosling, W.D., Lézine, A.-M., Scott, L. (Eds.), Quaternary Vegetation Dynamics – the African Pollen Database. CRC Press, London, pp. 301–308.

Duane, A., Castellnou, M., Brotons, L., 2021. Towards a comprehensive look at global drivers of novel extreme wildfire events. Climatic Change 165, 43.

DWD Climate Data Center, 2020. Recent and Historical Dataset: Monthly Mean Air Temperature for Station George Airport (CDC-ID 68828) Worldwide, Version Recent. https://opendata.dwd.de/climate_environment/CDC/observations_global/CLIMAT/. (Accessed 1 July 2020).

Engelbrecht, C.J., Landman, W.A., 2016. Interannual variability of seasonal rainfall over the Cape south coast of South Africa and synoptic type association. Clim. Dynam. 47, 295–313.

Engelbrecht, C.J., Landman, W.A., Engelbrecht, F.A., Malherbe, J., 2015. A synoptic decomposition of rainfall over the Cape south coast of South Africa. Clim. Dynam. 44, 2589–2607.

ESRI Inc., 2022. World Ocean Base. Esri, Garmin, GEBCO, NOAA NGDC, and Other Contributors.

Favre, A., Hewitson, B., Lennard, C., Cerezo-Mota, R., Tadross, M., 2013. Cut-off Lows in the South Africa region and their contribution to precipitation. Clim. Dynam. 41, 2331–2351.

Fick, S.E., Hijmans, R.J., 2017. WorldClim 2: new 1-km spatial resolution climate surfaces for global land areas. Int. J. Climatol. 37, 4302–4315.

Finch, J.M., Hill, T.R., Meadows, M.E., Lodder, J., Bodmann, L., 2022. Fire and montane vegetation dynamics through successive phases of human occupation in the northern Drakensberg, South Africa. Quat. Int. 611–612, 66–76.

Fine, P.M., Cass, G.R., Simoneit, B.R.T., 2001. Chemical characterization of fine particle emissions from fireplace combustion of woods grown in the northeastern United States. Environ. Sci. Technol. 35, 2665–2675.

Fine, P.M., Cass, G.R., Simoneit, B.R.T., 2002. Chemical characterization of fine particle emissions from the fireplace combustion of woods grown in the southern United States. Environ. Sci. Technol. 36, 1442–1451.

Frost, P.E., Kleyn, L.G., van den Dool, R., Burgess, M., Vhengani, L., Steenkamp, K., Wessels, K., 2018. The Elandskraal Fire, Knysna. A Data Driven Analysis. CSIR Meraka Institute, Brummeria, p. 73.

Gamarra, B., Sachse, D., Kahmen, A., 2016. Effects of leaf water evaporative ^{2}H-enrichment and biosynthetic fractionation on leaf wax *n*-alkane δ^{2}H values in C3 and C4 grasses. Plant, Cell Environ. 39, 2390–2403. https://doi.org/10.1111/pce.12789.

Garrigues, P., Budzinski, H., Manitz, M.P., Wise, S.A., 1995. Pyrolytic and petrogenic inputs in recent sediments: a definitive signature through phenanthrene and chrysene compound distribution. Polycycl. Aromat. Comp. 7, 275–284.

Geldenhuys, C.J., 1988. Phytogeography of the southern Cape forest flora. FRD Occasional report 45, 158–181.

Geldenhuys, C.J., 1994. Bergwind fires and the location pattern of forest patches in the southern Cape landscape, South Africa. J. Biogeogr. 21, 49–62.

Geppert, M., Hartmann, K., Kirchner, I., Pfahl, S., Struck, U., Riedel, F., 2022. Precipitation over southern Africa: moisture sources and isotopic composition. J. Geophys. Res. Atmos. 127, e2022JD037005.

Gessler, A., Brandes, E., Buchmann, N., Helle, G., Rennenberg, H., Barnard, R.L., 2009. Tracing carbon and oxygen isotope signals from newly assimilated sugars in the leaves to the tree-ring archive. Plant Cell Environ. 32, 780–795.

Gonçalves, C., Alves, C., Evtyugina, M., Mirante, F., Pio, C., Caseiro, A., Schmidl, C., Bauer, H., Carvalho, F., 2010. Characterisation of PM10 emissions from woodstove combustion of common woods grown in Portugal. Atmos. Environ. 44, 4474–4480.

Haberzettl, T., Baade, J., Compton, J., Daut, G., Dupont, L., Finch, J., Frenzel, P., Green, A., Hahn, A., Hebbeln, D., Helmschrot, J., Humphries, M., Kasper, T., Kirsten, K., Mäusbacher, R., Meadows, M., Meschner, S., Quick, L., Schefuß, E., Wündsch, M., Zabel, M., 2014. Paleoenvironmental investigations using a combination of terrestrial and marine sediments from South Africa - the RAIN (Regional Archives for Integrated iNvestigations) approach. Zentralbl. Geol. Paläontol. Teil 2014, 55–73.

Hahn, A., Schefuß, E., Andò, S., Cawthra, H.C., Frenzel, P., Kugel, M., Meschner, S., Mollenhauer, G., Zabel, M., 2017. Southern Hemisphere anticyclonic circulation drives oceanic and climatic conditions in late Holocene southernmost Africa. Clim. Past 13, 649–665.

Hanke, U.M., Eglinton, T.I., Braun, A.L.L., Reddy, C.M., Wiedemeier, D.B., Schmidt, M. W.I., 2016. Decoupled sedimentary records of combustion: causes and implications. Geophys. Res. Lett. 43, 5098–5108.

Harris, C., Burgers, C., Miller, J., Rawoot, F., 2010. O- and H-isotope record of Cape Town rainfall from 1996 to 2008, and its application to recharge studies of Table Mountain groundwater, South Africa. S. Afr. J. Geol. 113, 33–56.

Hennebelle, A., Aleman, J.C., Ali, A.A., Bergeron, Y., Carcaillet, C., Grondin, P., Landry, J., Blarquez, O., 2020. The reconstruction of burned area and fire severity using charcoal from boreal lake sediments. Holocene 30, 1400–1409.

Hepp, J., Mayr, C., Rozanski, K., Schäfer, I.K., Tuthorn, M., Glaser, B., Juchelka, D., Stichler, W., Zech, R., Zech, M., 2021. Validation of a coupled $\delta^{2}H_{n\text{-alkane}}$-$\delta^{18}O_{sugar}$ paleohygrometer approach based on a climate chamber experiment. Biogeosciences 18, 5363–5380.

Hepp, J., Schäfer, I.K., Lanny, V., Franke, J., Bliedtner, M., Rozanski, K., Glaser, B., Zech, M., Eglinton, T.I., Zech, R., 2020. Evaluation of bacterial glycerol dialkyl glycerol tetraether and ^{2}H–^{18}O biomarker proxies along a central European topsoil transect. Biogeosciences 17, 741–756.

Hepp, J., Tuthorn, M., Zech, R., Mügler, I., Schlütz, F., Zech, W., Zech, M., 2015. Reconstructing lake evaporation history and the isotopic composition of precipitation by a coupled δ^{18}O–δ^{2}H biomarker approach. J. Hydrol. 529, 622–631.

Hepp, J., Wüthrich, L., Bromm, T., Bliedtner, M., Schäfer, I.K., Glaser, B., Rozanski, K., Sirocko, F., Zech, R., Zech, M., 2019. How dry was the Younger Dryas? Evidence from a coupled δ^{2}H–δ^{18}O biomarker paleohygrometer applied to the Gemündener Maar sediments, Western Eifel, Germany. Clim. Past 15, 713–733.

Hepp, J., Zech, R., Rozanski, K., Tuthorn, M., Glaser, B., Greule, M., Keppler, F., Huang, Y., Zech, W., Zech, M., 2017. Late Quaternary relative humidity changes from Mt. Kilimanjaro, based on a coupled ^{2}H-^{18}O biomarker paleohygrometer approach. Quat. Int. 438, 116–130. Part B.

Horita, J., Wesolowski, D.J., 1994. Liquid-vapor fractionation of oxygen and hydrogen isotopes of water from the freezing to the critical temperature. Geochem. Cosmochim. Acta 58, 3425–3437.

Illenberger, W.K., 1996. The geomorphologic evolution of the Wilderness dune cordons, South Africa. Quat. Int. 33, 11–20.

IPCC, 2021. Climate Change 2021: the Physical Science Basis. Contribution of Working Group I to the Sixth Assessment Report of the Intergovernmental Panel on Climate Change. Cambridge University Press, Cambridge.

Irving, S.J.E., 1998. Late Quaternary Palaeoenvironments at Vankervelsvlei, Near Knysna, South Africa, Master Thesis. University of Cape Town, Rondebosch.

Irving, S.J.E., Meadows, M.E., 1997. Radiocarbon chronology and organic matter accumulation at Vankervelsvlei, near Knysna, South Africa. S. Afr. Geogr. J. 79, 101–105.

Johnsen, A.R., Wick, L.Y., Harms, H., 2005. Principles of microbial PAH-degradation in soil. Environ. Pollut. 133, 71–84.

Johnson, M.R., Anhausser, C.R., Thomas, R.J., 2006. The Geology of South Africa. Geological Society of South Africa, Johannesburg/Council for Geoscience, Pretoria.

Jolly, W.M., Cochrane, M.A., Freeborn, P.H., Holden, Z.A., Brown, T.J., Williamson, G.J., Bowman, D.M.J.S., 2015. Climate-induced variations in global wildfire danger from 1979 to 2013. Nat. Commun. 6, 7537.

Kappenberg, A., Braun, M., Amelung, W., Lehndorff, E., 2019. Fire condensates and charcoals: chemical composition and fuel source identification. Org. Geochem. 130, 43–50.

Karp, A.T., Behrensmeyer, A.K., Freeman, K.H., 2018. Grassland fire ecology has roots in the late Miocene. Proc. Natl. Acad. Sci. USA 115, 12130–12135.

Karp, A.T., Holman, A.I., Hopper, P., Grice, K., Freeman, K.H., 2020. Fire distinguishers: refined interpretations of polycyclic aromatic hydrocarbons for paleo-applications. Geochem. Cosmochim. Acta 289, 93–113.

Karp, A.T., Uno, K.T., Polissar, P.J., Freeman, K.H., 2021. Late miocene C4 grassland fire feedbacks on the Indian subcontinent. Paleoceanogr. Paleoclimatol. 36, e2020PA004106.

Kim, E.J., Choi, S.-D., Chang, Y.-S., 2011. Levels and patterns of polycyclic aromatic hydrocarbons (PAHs) in soils after forest fires in South Korea. Environ. Sci. Pollut. Control Ser. 18, 1508–1517.

Kirsten, K.L., Haberzettl, T., Wündsch, M., Frenzel, P., Meschner, S., Smit, A.J., Quick, L. J., Mäusbacher, R., Meadows, M.E., 2018. A multiproxy study of the ocean-atmospheric forcing and the impact of sea-level changes on the southern Cape coast, South Africa during the Holocene. Palaeogeogr. Palaeoclimatol. Palaeoecol. 496, 282–291.

Kirsten, K.L., Pretorius, L., Meadows, M.E., Weij, R., Aquino-López, M., Antonopoulos, H. G., Dubazana, Y., Qadeer, A., Finch, J., Bao, K., 2023. The depositional history of the Knysna estuary since European colonization in the context of sea level and human impacts. Frontiers in Ecology and Evolution 11, 1120460.

Kraaij, T., Baard, J.A., Arndt, J., Vhengani, L., van Wilgen, B.W., 2018. An assessment of climate, weather, and fuel factors influencing a large, destructive wildfire in the Knysna region, South Africa. Fire Ecology 14, 4.

Kraaij, T., Baard, J.A., Cowling, R.M., van Wilgen, B.W., Das, S., 2013a. Historical fire regimes in a poorly understood, fire-prone ecosystem: eastern coastal fynbos. Int. J. Wildland Fire 22, 277–287.

Kraaij, T., Cowling, R.M., van Wilgen, B.W., 2013b. Lightning and fire weather in eastern coastal fynbos shrublands: seasonality and long-term trends. Int. J. Wildland Fire 22, 288–295.

Kraaij, T., Msweli, S.T., Potts, A.J., 2022. Fuel trait effects on flammability of native and invasive alien shrubs in coastal fynbos and thicket (Cape Floristic Region). PeerJ 10, e13765.

Kraaij, T., van Wilgen, B.W., 2014. Drivers, ecology, and management of fire in fynbos. In: Allsopp, N., Colville, J.F., Verboom, G.A. (Eds.), Fynbos: Ecology, Evolution, and Conservation of a Megadiverse Region. Oxford University Press, Oxford, pp. 47–72.

Lehmann, M.M., Gamarra, B., Kahmen, A., Siegwolf, R.T.W., Saurer, M., 2017. Oxygen isotope fractionations across individual leaf carbohydrates in grass and tree species. Plant, Cell Environ. 40, 1658–1670.

Lehndorff, E., Wolf, M., Litt, T., Brauer, A., Amelung, W., 2015. 15,000 years of black carbon deposition – a post-glacial fire record from maar lake sediments (Germany). Quat. Sci. Rev. 110, 15–22.

Lemma, B., Bittner, L., Glaser, B., Kebede, S., Nemomissa, S., Zech, W., Zech, M., 2021. $\delta^2H_{n\text{-alkane}}$ and $\delta^{18}O_{sugar}$ biomarker proxies from leaves and topsoils of the Bale Mountains, Ethiopia, and implications for paleoclimate reconstructions. Biogeochemistry 153, 135–153.

Lima, A.L.C., Farrington, J.W., Reddy, C.M., 2005. Combustion-derived polycyclic aromatic hydrocarbons in the environment—a review. Environ. Forensics 6, 109–131.

Liu, H., Liu, W., 2019. Hydrogen isotope fractionation variations of *n*-alkanes and fatty acids in algae and submerged plants from Tibetan Plateau lakes: implications for palaeoclimatic reconstruction. Sci. Total Environ. 695, 133925.

Liu, J., Jiang, C., Wu, H., Guo, L., Zhang, H., Zhao, Y., 2023. Controls on leaf water hydrogen and oxygen isotopes: a local investigation across seasons and altitude. Hydrol. Earth Syst. Sci. 27, 599–612.

Loehle, C., 2007. A 2000-year global temperature reconstruction based on non-treering proxies. Energy Environ. 18, 1049–1058.

Long, C.J., Whitlock, C., Bartlein, P.J., Millspaugh, S.H., 1998. A 9000-year fire history from the Oregon Coast Range, based on a high-resolution charcoal study. Can. J. For. Res. 28, 774–787.

MacPherson, A.J., Gillson, L., Hoffman, M.T., 2019. Between- and within-biome resistance and resilience at the fynbos-forest ecotone, South Africa. Holocene 29, 1801–1816.

Mandiola, S.R., Grundling, A.T., Grundling, P.-L., van der Plicht, J., van der Waal, B.C. W., Grootjans, A.P., 2021. Ecohydrological analysis of a South African through-flow mire: Vankervelsvlei revisited. Mires Peat 27, 1–14.

Martin, A.R.H., 1968. Pollen analysis of Groenvlei lake sediments Knysna (South Africa). Rev. Palaeobot. Palynol. 7, 107–144.

McGrath, T.E., Chan, W.G., Hajaligol, M.R., 2003. Low temperature mechanism for the formation of polycyclic aromatic hydrocarbons from the pyrolysis of cellulose. J. Anal. Appl. Pyrol. 66, 51–70.

Merlivat, L., 1978. Molecular diffusivities of $H_2\,^{16}O$, $HD^{16}O$, and $H_2\,^{18}O$ in gases. J. Chem. Phys. 69, 2864–2871.

Meyers, P.A., 2003. Applications of organic geochemistry to paleolimnological reconstructions: a summary of examples from the Laurentian Great Lakes. Org. Geochem. 34, 261–289.

Miller, C., Finch, J., Hill, T., Peterse, F., Humphries, M., Zabel, M., Schefuß, E., 2019. Late Quaternary climate variability at Mfabeni peatland, eastern South Africa. Clim. Past 15, 1153–1170.

Miller, D.R., Castañeda, I.S., Bradley, R.S., MacDonald, D., 2017. Local and regional wildfire activity in central Maine (USA) during the past 900 years. J. Paleolimnol. 58, 455–466.

Milton, S.J., Petersen, H., Nampa, G., van der Merwe, H., Henschel, J.R., 2022. Drought as a driver of vegetation change in Succulent Karoo rangelands, South Africa. Afr. J. Range Forage Sci. 40, 181–195.

Msweli, S.T., Potts, A.J., Fritz, H., Kraaij, T., 2020. Fire weather effects on flammability of indigenous and invasive alien plants in coastal fynbos and thicket shrublands (Cape Floristic Region). PeerJ 8, e10161.

Mucina, L., Rutherford, M.C., 2006. The Vegetation of South Africa, Lesotho and Swaziland. SANBI, Pretoria.

NASA, J.P.L., 2013. NASA Shuttle Radar Topography Mission Global 1 Arc Second [Data Set]. NASA EOSDIS Land Processes DAAC. https://doi.org/10.5067/MEaSUREs/SRTM/SRTMGL1.003 from. (Accessed 29 December 2020).

Norström, E., Neumann, F.H., Scott, L., Smittenberg, R.H., Holmstrand, H., Lundqvist, S., Snowball, I., Sundqvist, H.S., Risberg, J., Bamford, M., 2014. Late Quaternary vegetation dynamics and hydro-climate in the Drakensberg, South Africa. Quat. Sci. Rev. 105, 48–65.

Oros, D.R., Abas, M.R.b., Omar, N.Y.M.J., Rahman, N.A., Simoneit, B.R.T., 2006. Identification and emission factors of molecular tracers in organic aerosols from biomass burning: Part 3. Grasses. Appl. Geochem. 21, 919–940.

Oros, D.R., Simoneit, B.R.T., 2001a. Identification and emission factors of molecular tracers in organic aerosols from biomass burning Part 1. Temperate climate conifers. Appl. Geochem. 16, 1513–1544.

Oros, D.R., Simoneit, B.R.T., 2001b. Identification and emission factors of molecular tracers in organic aerosols from biomass burning Part 2. Deciduous trees. Appl. Geochem. 16, 1545–1565.

Poster, D.L., Lopez de Alda, M.J., Schantz, M.M., Sander, L.C., Wise, S.A., Vangel, M.G., 2003. Development and analysis of three diesel particulate-related standard reference materials for the determination of chemical, physical, and biological characteristics. Polycycl. Aromat. Comp. 23, 141–191.

Power, M.J., Marlon, J., Ortiz, N., Bartlein, P.J., Harrison, S.P., Mayle, F.E., Ballouche, A., Bradshaw, R.H.W., Carcaillet, C., Cordova, C., Mooney, S., Moreno, P. I., Prentice, I.C., Thonicke, K., Tinner, W., Whitlock, C., Zhang, Y., Zhao, Y., Ali, A.A., Anderson, R.S., Beer, R., Behling, H., Briles, C., Brown, K.J., Brunelle, A., Bush, M., Camill, P., Chu, G.Q., Clark, J., Colombaroli, D., Connor, S., Daniau, A.L., Daniels, M., Dodson, J., Doughty, E., Edwards, M.E., Finsinger, W., Foster, D., Frechette, J., Gaillard, M.J., Gavin, D.G., Gobet, E., Haberle, S., Hallett, D.J., Higuera, P., Hope, G., Horn, S., Inoue, J., Kaltenrieder, P., Kennedy, L., Kong, Z.C., Larsen, C., Long, C.J., Lynch, J., Lynch, E.A., McGlone, M., Meeks, S., Mensing, S., Meyer, G., Minckley, T., Mohr, J., Nelson, D.M., New, J., Newnham, R., Noti, R., Oswald, W., Pierce, J., Richard, P.J.H., Rowe, C., Sanchez Goñi, M.F., Shuman, B.N., Takahara, H., Toney, J., Turney, C., Urrego-Sanchez, D.H., Umbanhowar, C., Vandergoes, M., Vanniere, B., Vescovi, E., Walsh, M., Wang, X., Williams, N., Wilmshurst, J., Zhang, J.H., 2008. Changes in fire regimes since the Last Glacial Maximum: an assessment based on a global synthesis and analysis of charcoal data. Clim. Dynam. 30, 887–907.

Quick, L.J., Carr, A.S., Meadows, M.E., Boom, A., Bateman, M.D., Roberts, D.L., Reimer, P.J., Chase, B.M., 2015. A late Pleistocene–Holocene multi-proxy record of palaeoenvironmental change from Still Bay, southern Cape Coast, South Africa. J. Quat. Sci. 30, 870–885.

Quick, L.J., Chase, B.M., Wündsch, M., Kirsten, K., Chevalier, M., Mäusbacher, R., Meadows, M., Haberzettl, T., 2018. A high-resolution record of Holocene climate and vegetation dynamics from the southern Cape coast of South Africa: pollen and microcharcoal evidence from Eilandvlei. J. Quat. Sci. 33, 1–14.

Quick, L.J., Meadows, M.E., Bateman, M.D., Kirsten, K.L., Mäusbacher, R., Haberzettl, T., Chase, B.M., 2016. Vegetation and climate dynamics during the last glacial period in the fynbos-afrotemperate forest ecotone, southern Cape, South Africa. Quat. Int. 404, 136–149. Part B.

Ratnam, J.V., Behera, S.K., Masumoto, Y., Yamagata, T., 2014. Remote effects of El Niño and modoki events on the austral summer precipitation of southern Africa. J. Clim. 27, 3802–3815.

Rein, B., Lückge, A., Reinhardt, L., Sirocko, F., Wolf, A., Dullo, W.-C., 2005. El Niño variability off Peru during the last 20,000 years. Paleoceanography 20, PA4003.

Rein, B., Lückge, A., Sirocko, F., 2004. A major Holocene ENSO anomaly during the Medieval period. Geophys. Res. Lett. 31, L17211.

Rogge, W.F., Hildemann, L.M., Mazurek, M.A., Cass, G.R., 1998. Sources of fine organic aerosol. 9. Pine, oak, and synthetic log combustion in residential fireplaces. Environ. Sci. Technol. 32, 13–22.

Sachse, D., Billault, I., Bowen, G.J., Chikaraishi, Y., Dawson, T.E., Feakins, S.J., Freeman, K.H., Magill, C.R., McInerney, F.A., van der Meer, M.T.J., Polissar, P., Robins, R.J., Sachs, J.P., Schmidt, H.L., Sessions, A.L., White, J.W.C., West, J.B., Kahmen, A., 2012. Molecular paleohydrology: interpreting the hydrogen- isotopic composition of lipid biomarkers from photosynthesizing organisms. Annu. Rev. Earth Planet Sci. 40, 221–249.

Schmidt, H.-L., Werner, R.A., Roßmann, A., 2001. 18O Pattern and biosynthesis of natural plant products. Phytochemistry 58, 9–32.

Scott, L., Lee-Thorp, J.A., 2004. Holocene climatic trends and rhythms in southern Africa. In: Battarbee, R.W., Gasse, F., Stickley, C.E. (Eds.), Past Climate Variability through Europe and Africa. Springer, Dordrecht, pp. 69–91.

Sessions, A.L., Burgoyne, T.W., Schimmelmann, A., Hayes, J.M., 1999. Fractionation of hydrogen isotopes in lipid biosynthesis. Org. Geochem. 30, 1193–1200.

Sjöström, J.K., Martínez Cortizas, A., Nylund, A., Hardman, A., Kaal, J., Smittenberg, R. H., Risberg, J., Schillereff, D., Norström, E., 2023. Complex evolution of Holocene hydroclimate, fire and vegetation revealed by molecular, minerogenic and biogenic proxies, Marais Geluk wetland, eastern Free State, South Africa. Quat. Sci. Rev. 314, 108216.

Sternberg, d.L., 1989. Oxygen and Hydrogen Isotope Ratios in Plant Cellulose: Mechanisms and Applications. In: Rundel, P.W., Ehleringer, J.R., Nagy, K.A. (Eds.), Stable Isotopes in Ecological Research. Springer, New York, New York, NY, pp. 124–141.

Sternberg, L., Deniro, M.J., Savidge, R.A., 1986. Oxygen isotope exchange between metabolites and water during biochemical reactions leading to cellulose synthesis. Plant Physiol. 82, 423–427.

Stogiannidis, E., Laane, R., 2015. Source characterization of polycyclic aromatic hydrocarbons by using their molecular indices: an overview of possibilities. In: Whitacre, D.M. (Ed.), Reviews of Environmental Contamination and Toxicology. Springer International Publishing, Cham, pp. 49–133.

Strobel, P., 2022. Late Quaternary Climate and Environmental Reconstruction Based on Lake and Peat Sediments from the Central Southern Cape Region of South Africa, Department of Physical Geography. Friedrich Schiller University Jena, Jena, p. 172.

Strobel, P., Bliedtner, M., Carr, A.S., Frenzel, P., Klaes, B., Salazar, G., Struck, J., Szidat, S., Zech, R., Haberzettl, T., 2021. Holocene sea level and environmental change at the southern Cape – an 8.5 kyr multi-proxy paleoclimate record from lake Voëlvlei, South Africa. Clim. Past 17, 1567–1586.

Strobel, P., Bliedtner, M., Carr, A.S., Struck, J., Du Plessis, N., Glaser, B., Meadows, M.E., Quick, L.J., Zech, M., Zech, R., Haberzettl, T., 2022a. Late Quaternary Investigation of Sediments from Vankervelsvlei. PANGAEA.

Strobel, P., Bliedtner, M., Carr, A.S., Struck, J., du Plessis, N., Glaser, B., Meadows, M.E., Quick, L.J., Zech, M., Zech, R., Haberzettl, T., 2022b. Reconstructing Late Quaternary precipitation and its source on the southern Cape coast of South Africa: a multi-proxy paleoenvironmental record from Vankervelsvlei. Quat. Sci. Rev. 284, 107467.

Strobel, P., Haberzettl, T., Bliedtner, M., Struck, J., Glaser, B., Zech, M., Zech, R., 2020. The potential of $\delta^2H_{n\text{-alkanes}}$ and $\delta^{18}O_{sugar}$ for paleoclimate reconstruction – a regional calibration study for South Africa. Sci. Total Environ. 716, 137045.

Strobel, P., Kasper, T., Frenzel, P., Schittek, K., Quick, L.J., Meadows, M.E., Mäusbacher, R., Haberzettl, T., 2019. Late Quaternary palaeoenvironmental change in the year-round rainfall zone of South Africa derived from peat sediments from Vankervelsvlei. Quat. Sci. Rev. 218, 200–214.

Talma, A.S., Vogel, J.C., 1992. Late quaternary paleotemperatures derived from a speleothem from Cango caves, Cape province, South Africa. Quat. Res. 37, 203–213.

Topness, R.G., Vachula, R.S., Balascio, N.L., D'Andrea, W.J., Pugsley, G., Dia, M., Tingley, M., Curtin, L., Wickler, S., Anderson, R.S., 2023. Northern Norway paleofire records reveal two distinct phases of early human impacts on fire activity. Holocene 33, 1304–1316.

Tuthorn, M., Zech, R., Ruppenthal, M., Oelmann, Y., Kahmen, A., del Valle, H.F., Eglinton, T., Rozanski, K., Zech, M., 2015. Coupling δ^2H and δ^{18}O biomarker results yields information on relative humidity and isotopic composition of precipitation - a climate transect validation study. Biogeosciences 12, 3913–3924.

Tyson, P.D., Preston-Whyte, R.A., 2000. The Weather and Climate of Southern Africa. Oxford University Press, Cape Town.

Vachula, R.S., Karp, A.T., Denis, E.H., Balascio, N.L., Canuel, E.A., Huang, Y., 2022. Spatially calibrating polycyclic aromatic hydrocarbons (PAHs) as proxies of area burned by vegetation fires: insights from comparisons of historical data and sedimentary PAH fluxes. Palaeogeogr. Palaeoclimatol. Palaeoecol. 596, 110995.

Vachula, R.S., Richter, N., 2018. Informing sedimentary charcoal-based fire reconstructions with a kinematic transport model. Holocene 28, 173–178.

Vachula, R.S., Russell, J.M., Huang, Y., Richter, N., 2018. Assessing the spatial fidelity of sedimentary charcoal size fractions as fire history proxies with a high-resolution sediment record and historical data. Palaeogeogr. Palaeoclimatol. Palaeoecol. 508, 166–175.

van Wilgen, B.W., Higgins, K.B., Bellstedt, D.U., 1990. The role of vegetation structure and fuel chemistry in excluding fire from forest patches in the fire-prone fynbos shrublands of South Africa. J. Ecol. 78, 210–222.

van Zinderen Bakker, E.M., 1976. The evolution of late Quaternary paleoclimates of Southern Africa. Palaeoecol. Afr. 9 9, 160–202.

van Zinderen Bakker, E.M., 1978. Quaternary vegetation changes in southern Africa. In: Werger, M.J.A. (Ed.), Biogeography and Ecology of Southern Africa. Springer Netherlands, Dordrecht, pp. 131–143.

Vicente, E.D., Vicente, A.M., Musa Bandowe, B.A., Alves, C.A., 2016. Particulate phase emission of parent polycyclic aromatic hydrocarbons (PAHs) and their derivatives (alkyl-PAHs, oxygenated-PAHs, azaarenes and nitrated PAHs) from manually and automatically fired combustion appliances. Air Quality, Atmosphere & Health 9, 653–668.

Wang, Z., Bi, X., Sheng, G., Fu, J., 2009. Characterization of organic compounds and molecular tracers from biomass burning smoke in South China I: broad-leaf trees and shrubs. Atmos. Environ. 43, 3096–3102.

Weldon, D., Reason, C.J.C., 2014. Variability of rainfall characteristics over the South Coast region of South Africa. Theor. Appl. Climatol. 115, 177–185.

Wilson, A.M., Latimer, A.M., Silander, J.A., Gelfand, A.E., de Klerk, H., 2010. A Hierarchical Bayesian model of wildfire in a Mediterranean biodiversity hotspot: implications of weather variability and global circulation. Ecol. Model. 221, 106–112.

Wündsch, M., Haberzettl, T., Cawthra, H.C., Kirsten, K.L., Quick, L.J., Zabel, M., Frenzel, P., Hahn, A., Baade, J., Daut, G., Kasper, T., Meadows, M.E., Mäusbacher, R., 2018. Holocene environmental change along the southern Cape coast of South Africa – insights from the Eilandvlei sediment record spanning the last 8.9 kyr. Global Planet. Change 163, 51–66.

Wündsch, M., Haberzettl, T., Kirsten, K.L., Kasper, T., Zabel, M., Dietze, E., Baade, J., Daut, G., Meschner, S., Meadows, M.E., Mäusbacher, R., 2016. Sea level and climate change at the southern Cape coast, South Africa, during the past 4.2 kyr. Palaeogeogr. Palaeoclimatol. Palaeoecol. 446, 295–307.

Yakir, D., DeNiro, M.J., 1990. Oxygen and hydrogen isotope fractionation during cellulose metabolism in lemna gibba L. Plant Physiol. 93, 325–332.

Yunker, M.B., Macdonald, R.W., Vingarzan, R., Mitchell, R.H., Goyette, D., Sylvestre, S., 2002. PAHs in the Fraser River basin: a critical appraisal of PAH ratios as indicators of PAH source and composition. Org. Geochem. 33, 489–515.

Zech, M., Glaser, B., 2009. Compound-specific δ^{18}O analyses of neutral sugars in soils using gas chromatography–pyrolysis–isotope ratio mass spectrometry: problems, possible solutions and a first application. Rapid Commun. Mass Spectrom. 23, 3522–3532.

Zech, M., Tuthorn, M., Detsch, F., Rozanski, K., Zech, R., Zöller, L., Zech, W., Glaser, B., 2013. A 220ka terrestrial δ^{18}O and deuterium excess biomarker record from an eolian permafrost paleosol sequence, NE-Siberia. Chem. Geol. 360–361, 220–230.

Zhang, W., Zhang, S., Wan, C., Yue, D., Ye, Y., Wang, X., 2008. Source diagnostics of polycyclic aromatic hydrocarbons in urban road runoff, dust, rain and canopy throughfall. Environ. Pollut. 153, 594–601.

Ziervogel, G., New, M., Archer van Garderen, E., Midgley, G., Taylor, A., Hamann, R., Stuart-Hill, S., Myers, J., Warburton, M., 2014. Climate change impacts and adaptation in South Africa. WIREs Climate Change 5, 605–620.

Zomer, R.J., Xu, J., Trabucco, A., 2022. Version 3 of the global aridity Index and potential evapotranspiration database. Sci. Data 9, 409.